

# Clinical Proton MR Spectroscopy in Central Nervous System Disorders<sup>1</sup>

Gülin Öz, PhD  
 Jeffrey R. Alger, MPhil, PhD  
 Peter B. Barker, MPhil  
 Robert Bartha, PhD  
 Alberto Bizzi, MD  
 Chris Boesch, MD, PhD  
 Patrick J. Bolan, PhD  
 Kevin M. Brindle, DPhil,  
 Cristina Cudalbu, PhD  
 Alp Dinçer, MD  
 Ulrike Dydak, PhD  
 Uzay E. Emir, PhD  
 Jens Frahm, PhD  
 Ramón Gilberto González, MD, PhD  
 Stephan Gruber, PhD  
 Rolf Gruetter, PhD  
 Rakesh K. Gupta, MD  
 Arend Heerschap, PhD  
 Anke Henning, PhD  
 Hoby P. Hetherington, PhD  
 Franklyn A. Howe, DPhil  
 Petra S. Hüppi, MD  
 Ralph E. Hurd, PhD  
 For the MRS Consensus Group<sup>2</sup>

A large body of published work shows that proton (hydrogen 1 [<sup>1</sup>H]) magnetic resonance (MR) spectroscopy has evolved from a research tool into a clinical neuroimaging modality. Herein, the authors present a summary of brain disorders in which MR spectroscopy has an impact on patient management, together with a critical consideration of common data acquisition and processing procedures. The article documents the impact of <sup>1</sup>H MR spectroscopy in the clinical evaluation of disorders of the central nervous system. The clinical usefulness of <sup>1</sup>H MR spectroscopy has been established for brain neoplasms, neonatal and pediatric disorders (hypoxia-ischemia, inherited metabolic diseases, and traumatic brain injury), demyelinating disorders, and infectious brain lesions. The growing list of disorders for which <sup>1</sup>H MR spectroscopy may contribute to patient management extends to neurodegenerative diseases, epilepsy, and stroke. To facilitate expanded clinical acceptance and standardization of MR spectroscopy methodology, guidelines are provided for data acquisition and analysis, quality assessment, and interpretation. Finally, the authors offer recommendations to expedite the use of robust MR spectroscopy methodology in the clinical setting, including incorporation of technical advances on clinical units.

© RSNA, 2014

*Online supplemental material is available for this article.*

<sup>1</sup>From the Center for Magnetic Resonance Research, University of Minnesota, 2021 6th St SE, Minneapolis, MN 55455 (G.O.) Received March 1, 2013; revision requested April 9; revision received July 30; accepted August 30; final version accepted August 27. Supported in part by the Swiss National Foundation (320030\_135743), Centre d'Imagerie Biomedicale (CIBM) of the University of Lausanne (UNIL), University de Geneva (UNIGE), University of Geneva Hospitals (HUG), Centre Hospitalier Universitaire Vaudois (CHUV), Ecole Polytechnique Fédérale de Lausanne (EPFL), Leenaards Foundation, and Louis-Jeantet Foundations. The Cancer Research UK (CR-UK) and Engineering and Physical Sciences Research Council (EPSRC) Cancer Imaging Centre received support from the CR-UK, EPSRC, Medical Research Council (MRC) and the Department of Health (England) Grant C1060/A10334; the National Institute for Health Research (NIHR) Biomedical Research Centre received funding from the National Health Service (NHS). **Address correspondence to G.O.** (e-mail: [gulin@cmr.umn.edu](mailto:gulin@cmr.umn.edu)).

<sup>2</sup>The complete list of authors and affiliations is at the end of this article.

© RSNA, 2014

Since the inception of magnetic resonance (MR) imaging in the 1980s, its employment in the diagnostic evaluation of the central nervous system (CNS) has had a major impact on patient management. With the advent of 1.5-T whole-body magnets, imaging of the CNS with unprecedented detail became possible by using the proton (hydrogen 1 [ $^1\text{H}$ ]) signal of water. Complementary to structural MR imaging,  $^1\text{H}$  MR spectroscopy has become an attractive approach with which to assess the levels of metabolites in normal and diseased CNS, especially as image-controlled, localized MR spectroscopy acquisition

techniques were developed. These early localization techniques included point-resolved spectroscopy (PRESS) (1,2) and stimulated echo acquisition mode (STEAM) (3), methods that are now widely used in clinical MR spectroscopy applications.

Preliminary studies revealed large differences in metabolite levels in acute stroke (4), chronic multiple sclerosis (5), and brain tumors compared with healthy brain (6). Although this work stimulated a surge of interest in  $^1\text{H}$  MR spectroscopy for diagnosing and assessing CNS disorders during the early days of the “Decade of the Brain” (1990–1999), many suboptimal patient studies (7) and the lack of consistent guidelines have led to a situation where, 20 years later, MR spectroscopy is still considered an “investigational technique” by some medical professionals and health care organizations. However, the ability to make an early, noninvasive diagnosis or to increase confidence in a suspected diagnosis is highly valued by patients and clinicians alike. As a result, an increasing number of imaging centers are incorporating MR spectroscopy into their clinical protocols for brain examinations in selected patients. To facilitate expanded use of MR spectroscopy in the clinical setting, this consensus statement encourages standardization of data acquisition, analysis, and reporting of results.

When assessing the impact of imaging techniques on health care (8), it is recommended that six criteria be evaluated: (a) technical feasibility, (b) diagnostic accuracy, (c) diagnostic impact, (d) therapeutic impact, (e) impact on outcome, and (f) societal impact (9). Although MR spectroscopy certainly fulfills the first two criteria, only a few studies have demonstrated that it has a wide impact on differential diagnosis, patient treatment, and outcome and none have measured the societal impact (ie, cost-benefit analysis) (8). Thus, it remains a challenge and task of high priority for the MR spectroscopy community to focus on studies that will quantify the extent to which MR spectroscopy improves diagnosis and leads to changes in patient treatment

resulting in improved outcomes. This consensus article has been produced by an international group of imaging scientists, neuroradiologists, neurologists, oncologists, and clinical neuroscientists from universities and MR vendors to document the impact of  $^1\text{H}$  MR spectroscopy in the clinical evaluation of disorders of the CNS. The MR Spectroscopy Consensus Group was formed from October 2011 to April 2012. The group drafted and finalized the manuscript jointly through e-mail correspondence and teleconferences with the group members and by means of two special interest group meetings held in connection to the 20th Scientific Meeting of the International Society for Magnetic Resonance in Medicine in May 2012 and the 21st Scientific Meeting of the International Society for Magnetic Resonance in Medicine in April 2013.

### Essentials

- Hydrogen 1 ( $^1\text{H}$ ) MR spectroscopy is complementary to MR imaging and adds clinically relevant information about metabolites in common brain abnormalities.
- MR spectroscopy is clinic-ready for diagnostic, prognostic, and treatment assessment of brain tumors, various neonatal and pediatric disorders (hypoxia-ischemia, inherited metabolic diseases, and traumatic brain injury), demyelinating disorders, and infectious brain lesions; it is expected to contribute to patient management in neurodegenerative disorders, epilepsy, and stroke.
- Provided that spectra are acquired reproducibly with a protocol that adheres to quality standards, clinical MR spectroscopy can be performed successfully at either 1.5 or 3.0 T.
- MR spectroscopy data acquisition and processing procedures must be harmonized across vendors for expanded clinical acceptance, as lack of standardization and quality assurance of MR spectroscopy data acquisition and analysis methods is a current impediment to widespread clinical use.

### $^1\text{H}$ MR Spectrum of the Brain: Metabolites and Their Biomarker Potential

MR spectroscopy provides a very different basic “readout” than MR imaging, namely a spectrum rather than an

#### Published online

10.1148/radiol.13130531 Content code: NR

Radiology 2014; 270:658–679

#### Abbreviations:

CNS = central nervous system  
 Cr = creatine  
 Gln = glutamine  
 Glu = glutamate  
 Lac = lactate  
 mlIns = *myo*-inositol  
 NAA = *N*-acetylaspartate  
 PRESS = point-resolved spectroscopy  
 SNR = signal-to-noise ratio  
 STEAM = stimulated echo acquisition mode  
 tCho = total choline  
 tCr = total creatine  
 TE = echo time  
 tNAA = NAA + *N*-acetylaspartylglutamate

#### Funding:

Supported in part by the National Center for Research Resources (P41 RR008079), National Institute of Biomedical Imaging and Bioengineering (P41 EB015894), and National Institute of Neurologic Disorders and Stroke (P30 NS076408).

Conflicts of interest are listed at the end of this article.

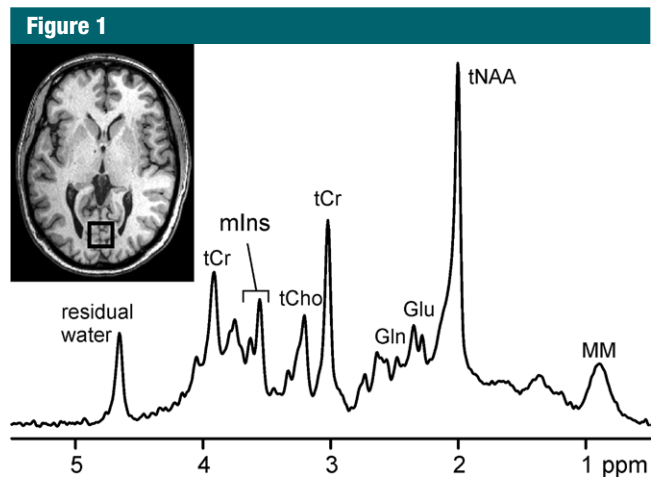


**Figure 1:**  $^1\text{H}$  MR spectrum acquired at 3.0 T from a volume of interest in occipital lobe ( $20 \times 20 \times 20 \text{ mm}^3$ , T1-weighted axial image) of healthy subject with the STEAM sequence (repetition time msec/echo time [TE] msec = 5000/8; 128 repetitions). *tNAA* = total *N*-acetylaspartate (NAA), *tCr* = total creatine (Cr), *tCho* = total choline, *Glu* = glutamate, *Gln* = glutamine, *mIns* = *myo*-inositol, *MM* = macromolecules.

image (Fig 1). Although MR images are conventionally displayed as gray-scale images that radiologists interpret by means of visual inspection of signal intensities and geometric structures, the MR spectrum consists of resonances or peaks that represent signal intensities as a function of frequency (commonly expressed as parts per million, a relative, magnetic field-independent frequency scale). Spectra are obtained either from one selected brain region in the case of single-voxel spectroscopy or from multiple brain regions in the case of MR spectroscopic imaging. The spectral data format has no antecedent in radiology, as MR images do in radiographic films, which may be one of the reasons for the relatively slow acceptance of MR spectroscopy in the clinical imaging community. Nevertheless, currently available analysis methods can help automatically and reliably quantify MR spectra in the clinical setting.

In vivo  $^1\text{H}$  MR spectroscopy focuses on carbon-bound protons in the 1–5 ppm range of the chemical shift scale (Fig 1) and can depict metabolites that are present at high enough concentrations (within the micromoles per gram range) and mobile on the MR spectroscopy time scale. These include the

neuronal metabolite NAA, the glial metabolite *mIns*, choline-containing compounds such as glycerophosphocholine and phosphocholine, neurotransmitters *Glu* and  $\gamma$ -aminobutyric acid, antioxidants glutathione and ascorbate, and other important metabolites such as *Cr*, phosphocreatine, *Gln*, and lactate (Lac) (10,11). Additional metabolites arise in specific clinical conditions, such as succinate and acetate in abscesses (12), lipids in various abnormalities (13,14), and even exogenous substances that cross the blood-brain barrier, such as propylene glycol after administration of some parenteral preparations (15) and ethanol after at least moderate alcohol consumption (16).

The number of quantifiable metabolites depends on the chosen pulse sequence and parameters, as well as the spectral resolution and signal-to-noise ratio (SNR), which are affected by many factors including the static magnetic field strength, quality of  $B_0$  field homogeneity, and radiofrequency coil used (17,18). The major singlet resonances originating from total MR spectroscopy-visible NAA (*tNAA*) (ie, NAA + *N*-acetylaspartylglutamate), *tCr* (ie, Cr + phosphocreatine), and *tCho* (ie, primarily phosphocholine + glycerophosphocholine) can be

quantified at all clinical magnetic field strengths and at almost all practical TEs up to 280 msec (19,20). At 1.5 T and short TEs (25–35 msec for PRESS, 20 msec or shorter for STEAM), *mIns* and combined *Glu* and *Gln* can also be quantified (21). At field strengths of 3.0 T and higher, additional metabolites are detected at short TEs (eg,  $\gamma$ -aminobutyric acid and glutathione) and the separation of *Glu* and *Gln* is feasible (22,23). Up to 18 metabolites can be quantified at short TEs and field strengths of 7.0 or 9.4 T (23–25).

A subset of the metabolites detectable by using MR spectroscopy may serve as biomarkers in the context of physiologic and pathologic states. For at least one MR spectroscopy-detected metabolite, NAA, evidence from cell (26), ex vivo brain (27), and histologic studies (28) show unequivocally that, in the mature CNS, NAA is present only in neurons, axons, and dendrites—not in glial cells. Together with  $^1\text{H}$  MR spectroscopy results of human brain ex vivo specimens (29) and in vivo data (30), these observations make a strong case that NAA is a biomarker for neuronal integrity. In addition, NAA levels may reflect mitochondrial (dys)function (31). *tNAA* (comprised primarily of NAA, with a small contribution from *N*-acetylaspartylglutamate) is therefore commonly used as a positive or negative in vivo biomarker either for the presence of viable neurons or the assessment of parenchymal damage. Elevated *mIns* is generally considered a marker for gliosis (32,33), and high *tCho* may be a marker for cellular proliferation, increased membrane turnover, or inflammation (13,29,34,35). Elevated Lac is indicative of anaerobic glycolysis and may be considered an unspecific MR spectroscopy biomarker for several abnormalities (36,37).

### MR Spectroscopy of CNS Disorders

Neurologic diseases affect as many as 1 billion people worldwide and are a major cause of disability and human suffering. Diagnosis is often complex, and the time window for effective therapy may be limited. MR imaging, with its excellent

soft-tissue contrast, is commonly the modality of choice for the detection of brain lesions. The morphologic details and the sensitivity to changes in content and physical properties of water are exquisite. However, conventional MR imaging is not able to depict changes in cell density, cell type, or biochemical composition—all of which can be investigated with MR spectroscopy. Furthermore, lesions of different underlying pathophysiology often manifest with a similar MR imaging appearance. Accordingly, MR imaging and MR spectroscopy are complementary tools for diagnosing disease and monitoring disease progression and response to therapy.

In the next sections, we will first report on the clinical impact of  $^1\text{H}$  MR spectroscopy in the evaluation of diseases in which it has already been demonstrated to be valuable and next on the potential clinical utility of MR spectroscopy in disorders where substantial research activity has occurred in the past 2 decades with consistent results across laboratories. The breakdown is based on (a) the demonstration of improved diagnostic accuracy of MR spectroscopy over other commonly used clinical imaging modalities, (b) the presence of disease-linked specific metabolites in the  $^1\text{H}$  MR spectrum, and (c) the demonstration of reduced need for invasive diagnostic procedures. In general, the “patient-ready” applications involve large disease effects detectable in an individual MR spectrum, whereas disorders for which  $^1\text{H}$  MR spectroscopy is expected to contribute to future patient management involve subtle spectroscopic changes that are more challenging to detect in individual cases. Table 1 summarizes the CNS disorder entities that are covered herein and lists metabolites of interest for these disorders.

#### Neurologic Diseases in Which $^1\text{H}$ MR Spectroscopy Is Valuable for Clinical Decision Making

##### Brain Tumors

Clinical decision making in neuro-oncology is achieved by a multidisciplinary team combining information from many sources, including MR imaging.

Although it plays a central role in the clinical management of patients with brain tumors, MR imaging alone cannot provide the answer to many important clinical questions. These include differentiating tumor from other focal lesions (giant demyelinating plaques, encephalitis), obtaining a definitive diagnosis of atypical ring-enhancing focal lesions (ie, high-grade gliomas, metastasis, lymphoma, and abscess), identifying the optimal biopsy sites in heterogeneous gliomas, monitoring the response to treatment, and differentiating between treatment-induced changes and recurrent tumor. MR spectroscopy can provide information in all of these key clinical areas, and it is increasingly being used as an adjunct to MR imaging.

The earliest reports in human brain tumors (6), together with work in vivo specimens (39,40) and cancer cells (41), demonstrated that MR spectroscopy offers great potential for noninvasive assessment of brain neoplasms. For example, MR spectroscopy in conjunction with perfusion imaging provided a sensitivity of 72% and a specificity of 92% in the differentiation of tumors from nonneoplastic lesions (42). Similarly, a sensitivity of 93% and a specificity of 60% were achieved when using these two methods for identifying high-versus low-grade gliomas, a substantial improvement in sensitivity over that with conventional MR imaging (43).

Large multicenter studies have determined the accuracy of single-voxel MR spectroscopy with pattern recognition algorithms for diagnosing brain tumor histology and grade (44–46). Short TE MR spectroscopy gives an accuracy of approximately 90% for all pairwise comparisons of the main adult tumor types (meningiomas, low-grade glioma, glioblastoma multiforme, metastases) except for glioblastoma multiforme versus metastasis, where the accuracy was 78% (44,46). Combining short and long TE MR spectroscopy gives a diagnostic accuracy for the main childhood brain tumor types (pilocytic astrocytoma, medulloblastoma, and ependymoma) of 98% (45). More recently, MR spectroscopy helped identify molecular

subtypes of gliomas with isocitrate dehydrogenase mutations, an example of molecular fingerprinting in vivo, on the basis of levels of 2-hydroxyglutarate (47). Few studies compared the diagnostic accuracy of MR spectroscopy with that of conventional MR imaging, but one study established added value for a decision support system constructed from multicenter data. Namely,  $^1\text{H}$  MR spectroscopy data improved low- and high-grade tumor prediction relative to MR imaging alone; the area under the receiver operating characteristic curve for low-grade tumors was 0.93 for MR imaging plus MR spectroscopy versus 0.81 for MR imaging alone, and the area under the receiver operating characteristic curve for high-grade tumors was 0.93 for MR imaging plus MR spectroscopy versus 0.85 for MR imaging alone (48). Elevated tCho along with decreased tNAA is typically regarded as a diagnostic feature of brain tumors (13) (Fig 2). In addition, the prominent signal at 1.3 ppm, which arises from lipids present in cytoplasmic droplets associated with necrosis or hypoxia, is generally associated with higher grade and poor survival (49–51) (Fig 2). Conversely, nonneoplastic lesions such as abscesses and tuberculomas often demonstrate elevated amino acids and lipids (52). Other metabolites observed in brain neoplasms include taurine in primitive neuroectodermal tumor (53), alanine in meningiomas (13), and glycine in high-grade pediatric tumors (54). If biopsy is needed for diagnosis, the tCho/tNAA ratio can help differentiate areas of solid tumor with the highest cell density from edema (55,56). The detection of an increased tCho/tNAA ratio in the peritumoral region further reflects tumor invasiveness and can thus be used to differentiate high-grade gliomas from brain metastases that exhibit a near-normal spectrum in the peritumoral region (57,58). MR spectroscopy has also been shown to have a decisive role in the diagnosis of low-grade versus high-grade tumors, as well as in the diagnosis of metastasis versus high-grade tumors, as part of a diagnostic work-up that includes conventional MR imaging

**Table 1**  
**MR Spectroscopy Methods Used to Image Brain Disorders and Metabolites of Interest for Each Disorder**

Disorder and MR Spectroscopy Method*	Location of VOI or ROI†	Metabolites of Interest‡
Suspected tumor > 10 mL at gadolinium-enhanced T1-weighted MR imaging or FLAIR MR imaging	VOI or ROI on the contrast-enhancing region of tumor if it exists, avoiding necrotic core, and on FLAIR abnormality for nonenhancing tumors	tNAA, tCho, tCr, Lac, mins, lipids
SVS, STE or LTE PRESS, STE STEAM	VOI or ROI on the contrast-enhancing region of tumor if it exists, avoiding necrotic core, and on FLAIR abnormality for nonenhancing tumors	tNAA, tCho, tCr, Lac
LTE MRSI		
Suspected tumor < 10 mL at gadolinium-enhanced T1-weighted MR imaging or FLAIR MR imaging	VOI or ROI on the contrast-enhancing region of tumor if it exists, avoiding necrotic core, and on FLAIR abnormality for nonenhancing tumors	tNAA, tCho, tCr, Lac, lipids
STE or LTE MRSI		
Suspected infective focal lesion	VOI within the lesion	Ac, Suc, Lac, lipids, amino acids (Ala, Leu, isoleu, Val)
SVS, STE or LTE PRESS		
Suspected metabolic disorder	VOI according to metabolic disorder, eg, in parietal cortex for Cr deficiencies, in basal ganglia for Leigh disease, white matter in most cases	tNAA, tCr, Lac, Gly, Ala, Pyr, Suc
SVS, STE or LTE PRESS, STE STEAM	Section through parietal cortex/white matter/basal ganglia	tNAA, tCr, Lac, Gly, Ala, Pyr, Suc
LTE MRSI		
Neonatal hypoxia-ischemia	VOI in basal ganglia	tNAA, tCr, Lac, MM
SVS, STE or LTE PRESS, STE STEAM		
Suspected demyelinating disorder	VOI in T2 hyperintense white matter lesion	tNAA, tCr, tCho, mins, MM
SVS, STE or LTE PRESS	Section covering T2 hyperintense white matter lesions	tNAA, tCr, tCho
LTE MRSI		
Multiple sclerosis	VOI within white matter lesion	tNAA, tCr, tCho, MM
SVS, STE or LTE PRESS	Section covering white matter including corpus callosum	tNAA, tCr, tCho
LTE MRSI		
Suspected dementia	VOIs in posterior cingulate and mesial temporal lobes	tNAA, tCr, tCho, mins, Glx
SVS, STE PRESS, STE STEAM	Section angulated along planum temporale and above the lateral ventricles	tNAA, tCho, tCr, (mins)
LTE MRSI		
Focal epilepsy	ROI best defined by clinical data	tNAA, tCr, tCho
LTE MRSI		
Mesial temporal lobe epilepsy	Bilateral voxels in mesial temporal structures, planum temporale angulation	tNAA, tCr, tCho
SVS, STE or LTE PRESS		
Ischemic lesion	VOI within reduced diffusion volume	tNAA, tCr, Lac, tCho
SVS, STE or LTE PRESS	Section through reduced diffusion volume	tNAA, tCr, Lac, tCho
LTE MRSI		

Note.—FLAIR = fluid-attenuated inversion recovery.

\* Clinically available MR spectroscopy methods that have been widely used for the abnormalities indicated are listed. Short TE is 25–35 msec for PRESS sequence and 20 msec for STEAM sequence. Long TE is 135–270 msec (typically only used for single-voxel spectroscopy). 144 msec is used for Lac inversion, however, precaution is required about chemical shift displacement errors at 3.0 T (38). LTE = long TE, MRSI = MR spectroscopic imaging, STE = short TE, SVS = single-voxel spectroscopy.

† ROI = region of interest, VOI = volume of interest.

‡ Note that mins, a combination of Glu and Gln (Glx), macromolecules (MM), and lipids are detected reliably with short TE sequences, whereas glycine (Gly) is detected reliably with long TE sequences. Ac = acetate, Ala = alanine, isoleu = isoleucine, Leu = leucine, Pyr = pyruvate, Suc = succinate, Val = valine.

Figure 2

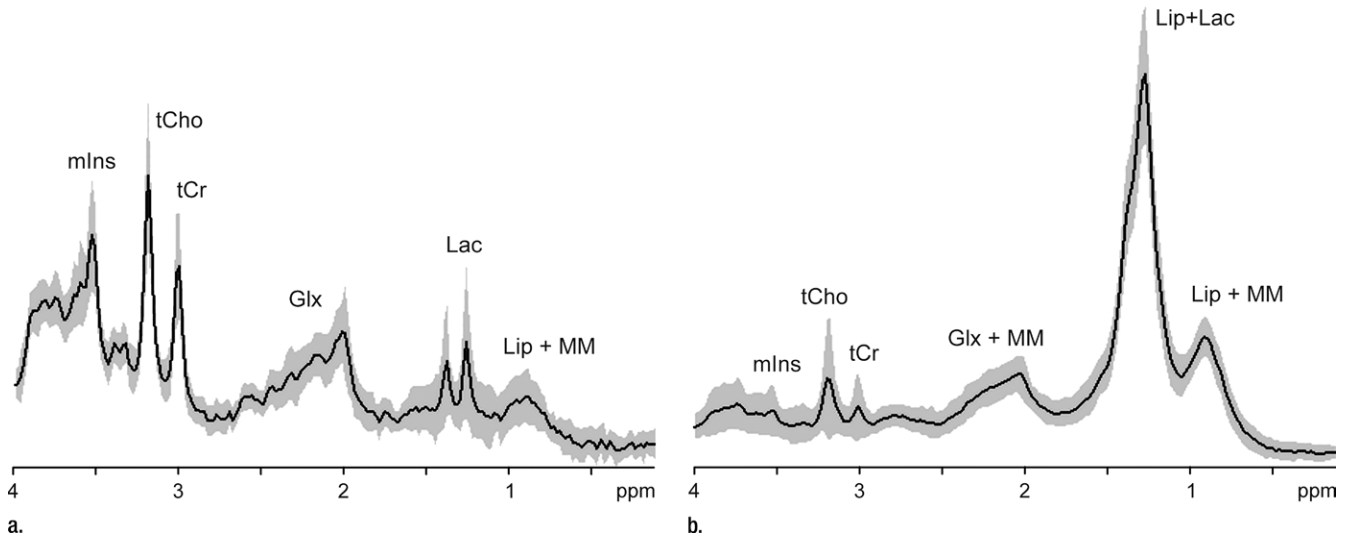


**Figure 2:** MR spectroscopy of astrocytomas. Average (solid line) and standard deviation (shaded area)  $^1\text{H}$  MR spectra (1.5 T, STEAM or PRESS, 2000/30, 128–256 repetitions per spectrum included in average) in World Health Organization (a) grade II ( $n = 14$ ) and (b) grade IV ( $n = 42$ ) astrocytomas. Characteristically elevated tCho/tCr ratio and absence of tNAA is apparent in both tumor spectra compared with that from normal brain (see Fig 1). Lac in low-grade tumor may be the result of hypoxia and/or a metabolic shift toward glycolysis, as is commonplace in cancer. In high-grade tumor, large macromolecule (MM) and lipid (Lip) signals (at chemical shifts 2.0, 1.3, and 0.9 ppm) are associated with necrosis. Glx = combination of Glu and Gln. (Reprinted, with permission, from reference 49.)

with gadolinium and diffusion-weighted and perfusion MR imaging (59).

MR spectroscopy may be used to determine prognosis and to guide treatment planning in oncology patients when surgery is not indicated, such as in diffuse brainstem gliomas and intramedullary tumors in the spinal cord (60). A tCho/tNAA peak amplitude ratio of at least 2.1 (either at single-voxel spectroscopy with a TE of 144 or 270 msec or at MR spectroscopic imaging with a TE of 280 msec) was found prognostic of unfavorable outcome in pediatric diffuse pontine gliomas (61). Prognostic MR spectroscopy markers are important for treatment stratification and can help identify patients who need more intensive treatment from the outset for some tumor types (47,62,63). These include the detection of 2-hydroxyglutarate in isocitrate dehydrogenase-1 mutated gliomas (47), citrate in proliferating pediatric astrocytomas (62), and highly MR spectroscopy-visible saturated lipids with elevated *scyllo*-inositol and low glutamine in high-risk pediatric brain tumors (64). A tCho/tNAA ratio of more than 2.1 at long

TE MR spectroscopic imaging has been used to identify regions of more aggressive phenotype within a heterogeneous glioblastoma multiforme to improve gamma knife radiosurgery (64).

For neurosurgical treatment planning, MR spectroscopy plays a role in differentiating areas of tumor from benign processes and, together with other MR imaging methods, in establishing their relationship to key normal brain structures (56), particularly in gliomas. Infiltrative gliomas extend well beyond the T2-defined main tumor bulk. One study reported that the MR spectroscopy-defined abnormal area was an average of 24% larger than that delineated by T2 hyperintensity and confirmed the accuracy of an elevated tCho/tNAA ratio with histologic and immunohistochemistry findings for tumor cells (65). Another study demonstrated increased mIns and Gln levels in the contralateral hemisphere of patients with untreated glioblastoma multiforme, a finding that was indicative of early neoplastic infiltration (66). In addition, gliomas of all grades may have intratumoral heterogeneity

(67), sometimes even despite apparent homogeneous imaging characteristics. It is common to find low-grade oligodendrogliomas with malignant imaging features, nonenhancing high-grade gliomas with benign imaging features, and focal areas of malignancy in low-grade gliomas. In low-grade gliomas, detection of areas with infiltrative tumor cells (close or distant to the main mass) is very important as these can be the primary sites of tumor recurrence. Delineation of tumor infiltration is an essential part of (a) preoperative decision making, (b) intraoperative MR imaging-guided resections, and (c) postoperative follow-up and application of additional therapies (post-surgery radiation and/or chemotherapy). MR spectroscopy was shown to spatially correlate with histologic type and grade and to reflect heterogeneity in brain tumors before surgery: A tCho/tNAA ratio greater than 2, a Lac/tNAA ratio greater than 0.25, and the presence of lipid at MR spectroscopic imaging with a long TE (144 msec) are characteristics of a high-grade tumor, allowing demarcation

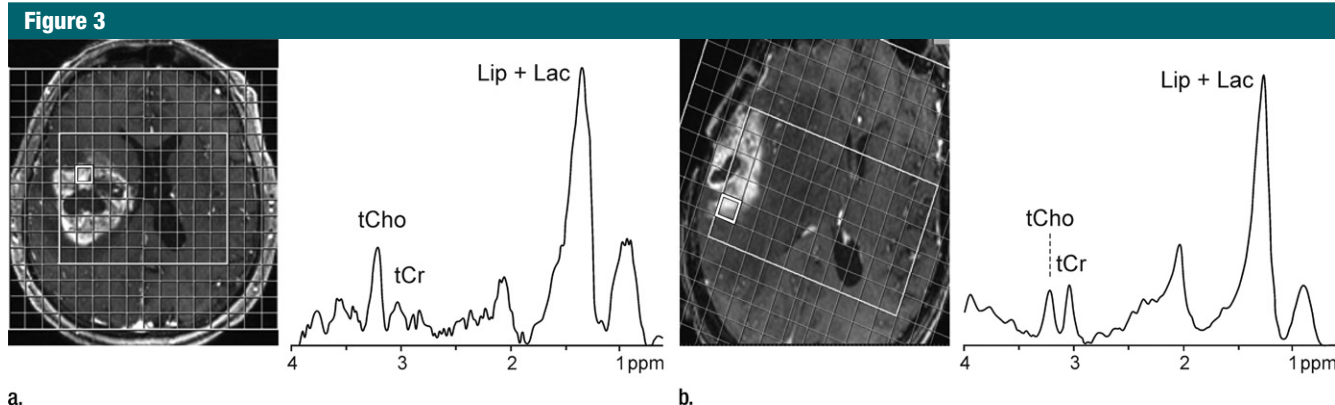


**Figure 3:**  $^1\text{H}$  MR spectroscopy in glioblastomas. Contrast-enhanced T1-weighted MR images and MR spectroscopy grid (3.0 T, PRESS, 1700/30, three repetitions, section thickness = 20 mm, matrix size =  $16 \times 16$ , total acquisition time = 6 minutes 46 seconds) are shown together with representative spectra from voxels in contrast-enhancing areas. **(a)** Image and spectrum from patient with recurrent glioblastoma multiforme exhibits elevated tCho/tCr ratio as well as elevated lipid (*Lip*) and Lac levels. **(b)** Image and spectrum from histologically proven case of postradiation injury exhibits markedly elevated lipid (*Lip*) and Lac levels along with normal-appearing tCho/tCr ratio.

of brain parenchyma adjacent to MR imaging–delineated tumor (56). In addition, recent intraoperative  $^1\text{H}$  MR spectroscopy at 3.0 T helped differentiate tumor from a nontumoral abnormality, as indicated by a high tCho/tCr ratio and the presence of Lac, in 57% of suspected cases and had a positive effect on surgical success and patient outcome (68).

MR spectroscopy can help avoid the incorrect diagnosis of tumor progression, which can lead to inappropriate surgery, other treatment, and patient distress in cases of posttreatment-induced changes that are ambiguous at conventional MR imaging. For example, the tCho/tNAA ratio was shown to reliably differentiate recurrent glioma from postradiation injury (69) (Fig 3). Similarly, MR spectroscopy (tCho/water), either alone or in combination with conventional MR imaging, can further contribute to the assessment of response to anticancer treatment (70). MR spectroscopy (tCho/tCr and tCho/tNAA) and dynamic susceptibility contrast MR imaging in isolation showed diagnostic accuracy of 84.6% and 86%, respectively; the accuracy increased to 93.3% when combined data were used for tumor regrowth and posttreatment injury (71). MR spectroscopy (tNAA/tCho ratio and tCho concentration) in combination with dynamic susceptibility

contrast MR imaging was reported to have 100% positive and negative predictive values for discriminating posttreatment change, which is more accurate than both conventional MR imaging (positive predictive value, 50%) and fluorine 18 deoxyglucose positron emission tomography (PET) (positive predictive value, 67%; negative predictive value, 60%) (72). However, dynamic susceptibility contrast MR imaging showed a substantial false-positive rate, which was not the case with MR spectroscopy—a finding that points to an incremental value of MR spectroscopy in separating tumor recurrence and posttreatment injury (72).

In summary, MR spectroscopy adds diagnostic and prognostic benefits to MR imaging and aids in treatment planning and monitoring of brain cancers.

#### Pediatric Disorders: Hypoxia-Ischemia, Inherited Metabolic Diseases, and Traumatic Brain Injury

$^1\text{H}$  MR spectroscopy was used for pediatric brain imaging as early as 1990–1991 (73–75), and it is part of routine imaging protocols in many specialized academic health centers and children's hospitals. For the newborn infant, quantitative assessment of cerebral Lac due to hypoxia-ischemia is one of the earliest imaging signs indicative of clinical brain injury (37,76) (Fig 4), and

persistence of high Lac is associated with poor outcome (77). MR spectroscopy can be used as a means to assess treatment efficacy of hypothermia, a proven neuroprotective treatment for perinatal asphyxia (78).

Although rare, inherited metabolic disorders are a significant disease entity in neuropediatrics. Clinical symptoms in certain inherited metabolic diseases are due to the accumulation of metabolites that are either neurotoxic or interfere with normal function. If the accumulating substance is visible at MR spectroscopy, its presence or elevation in the spectrum can be used for diagnosis. MR spectroscopy has proved clinically useful in neonates suspected of having metabolic disorders (79–81) owing to the unique ability to noninvasively detect the metabolic defect in vivo (82–85). For example, the presence of pyruvate (plus Lac and/or alanine) and succinate are early indicators of pyruvate and succinate dehydrogenase complex deficiencies, respectively (79,86–88). Detection of elevated glycine, in particular at long TEs, is clinically diagnostic in nonketotic hyperglycinemia (82), although intracerebral hemorrhage presents a confound in the interpretation of high glycine levels (89). A grossly elevated tNAA level is a diagnostic hallmark of Canavan disease (90).

In other inherited diseases, the reduction of metabolites owing to

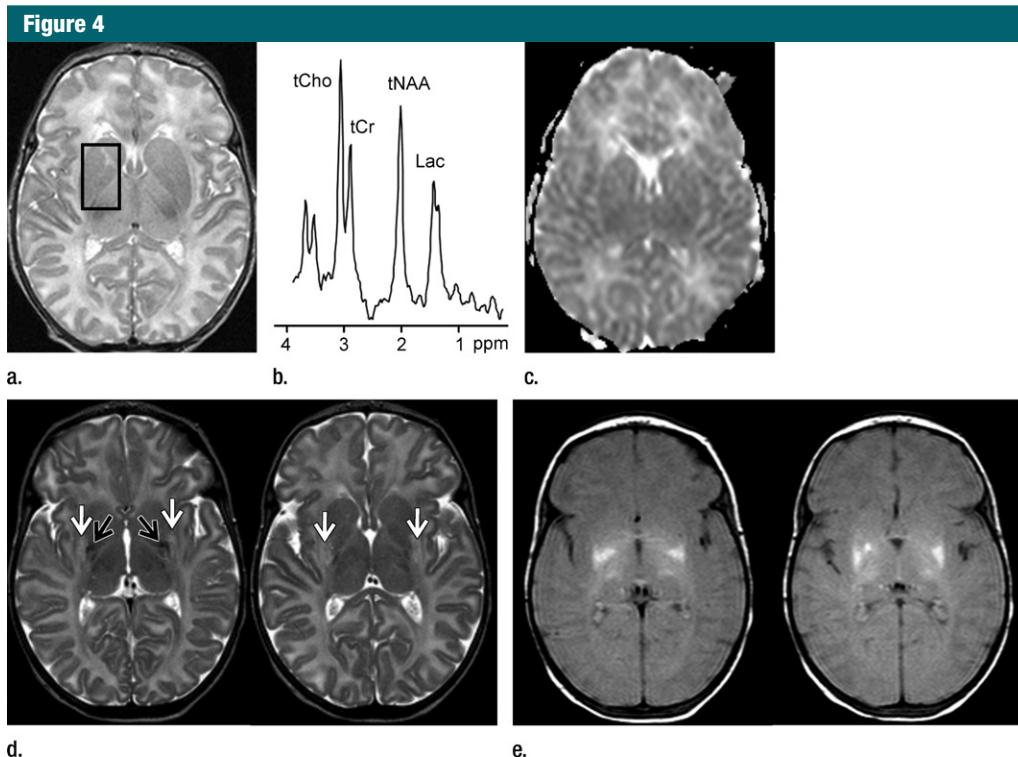


**Figure 4:**  $^1\text{H}$  MR spectroscopy in early assessment of perinatal hypoxia-ischemia in the newborn. MR imaging was performed (a–c) 12 hours and (d, e) 10 days after perinatal asphyxia. (a) Axial T2-weighted image shows no signal abnormalities, whereas (b) spectrum (1.5 T, PRESS, 1500/288, 192 repetitions) obtained from the right basal ganglia shows markedly increased Lac resonance with preserved tNAA, tCr, and tCho resonances. (c) Diffusion-weighted image (echo-planar imaging; 30 directions;  $b$  value, 700  $\text{sec}/\text{mm}^2$ ) with axial apparent diffusion coefficient map shows no diffusion abnormalities. (d) Axial T2-weighted images show areas of high (white arrows) and low (black arrows) signal intensity in putamen and thalamus, representing clear ischemohemorrhagic lesions. (e) Axial proton density images demonstrate prominent detection of lesion's extension. (Reprinted, with permission, from reference 76.)

decreased synthesis or transport can be detected with MR spectroscopy. An absent or severely reduced tCr level presents a limited differential diagnosis of three underlying genetic defects (91): The lowest tCr levels are observed in untreated children with a Cr synthesis defect (guanidinoacetate methyltransferase or arginine:glycine amidinotransferase deficiency), and treatment leads to at least partial normalization of cerebral tCr (92,93) (Fig 5). In males with a Cr-transporter deficiency, brain tCr concentrations are reduced by four- to fivefold compared with that in healthy control subjects. These patients do not benefit from Cr therapy either with or without additional arginine and glycine (94,95). The absence of tNAA owing to a defect in NAA synthesis (96) has been described in a case study (97).

More minor changes in single or multiple metabolites require careful quantification of the MR spectra and comparison with well-established normal values. It is quite challenging to obtain these data in the pediatric population owing to limitations associated with imaging healthy children, but they are particularly crucial because of developmental changes in metabolite levels (98). This challenge can be overcome by using normative data from children who undergo MR imaging and spectroscopy for the investigation of suspected neurologic conditions. This approach has proved useful in Hunter syndrome, a mucopolysaccharoidosis (99), and propionic acidaemia (100).

Traumatic brain injury is a major cause of disability and death among children younger than 14 years (101).

For effective clinical management, objective means to evaluate long-term outcome are required, especially for comatose patients. In a cohort of children with traumatic brain injury, a regression model, incorporating age, initial Glasgow coma scale, and presence of retinal hemorrhage and supplemented with tNAA/tCr ratio and MR spectroscopy-visible Lac within the 1st month after incidence, was shown to differentiate between good and poor outcomes (102). In pediatric near-drowning accidents, an MR spectroscopy index based on tNAA, Lac, and combined Glu and Gln was shown to correctly differentiate between good and poor outcomes—with no false-positive results (103). These data support the clinical utility of MR spectroscopy in combination

Figure 5

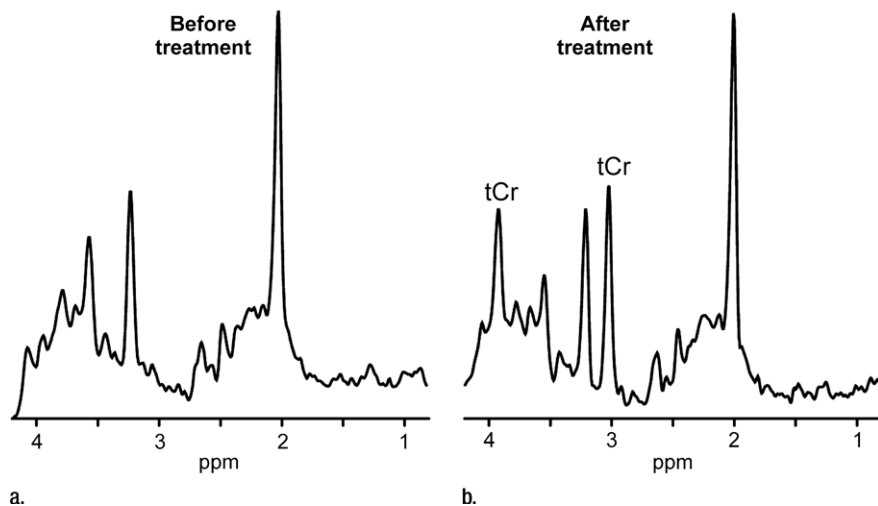


**Figure 5:**  $^1\text{H}$  MR spectroscopy of neurometabolic disorder. (a, b) White matter spectra (1.5 T, PRESS MR spectroscopic imaging, 3000/30, six weighted averages, nominal voxel size =  $10 \times 10 \times 15 \text{ mm}^3$ ) in girl with guanidinoacetate methyltransferase deficiency before treatment at age 3 years 2 months (a) and after 3.5 months of treatment with oral creatine supplementation (b). Resonance from creatine-containing metabolites (tCr) returned to normal in this region as well as in other investigated brain areas.

with clinical measures for predicting outcome.

### Demyelinating Diseases

MR spectroscopy plays an important role alone (104) or in addition to other semiquantitative MR techniques (105) in the differential diagnosis of hereditary leukoencephalopathies. MR spectroscopy provides valuable information about tissue pathophysiology for at least three different metabolic profiles: (a) hypomyelination, (b) white matter rarefaction, and (c) demyelination, which were differentiated with tCho/tCr and tNAA/tCr ratios in a study of 70 children (104).

Hematopoietic stem cell transplantation is currently the only treatment option for inherited demyelinating disorders such as X-linked adrenoleukodystrophy, metachromatic leukodystrophy, and globoid cell leukodystrophy (106). MR spectroscopy is used to monitor the onset of demyelination in neurologically asymptomatic patients with X-linked adrenoleukodystrophy with high genotypic variability (14,32,107). Interval elevation of mIns/tNAA and tCho/tNAA ratios in normal-appearing white matter at

follow-up is an indication for treatment with hematopoietic stem cell transplantation (Fig 6). Hematopoietic stem cell transplantation performed before substantial tissue degeneration as assessed with tNAA results in clinical stabilization (108). In patients who are newly diagnosed with juvenile or adult metachromatic leukodystrophy, a combination of MR imaging and MR spectroscopy can be used to judge the state of brain tissue inflammation (109,110). Although mIns is typically increased even in the early stages of metachromatic leukodystrophy, as long as tNAA is still within the normal range, hematopoietic stem cell transplantation is indicated (111,112).

The clinical use of MR spectroscopy in multiple sclerosis, an acquired demyelinating disease, remains limited despite the various insights into disease pathology that it has offered as well as its ability to assess the burden of axonal damage (113). MR spectroscopy of chronic multiple sclerosis plaques in white matter shows a consistently reduced tNAA/tCr ratio (5,35) and, sometimes, an elevated tCho/tCr ratio (35). Spectra from plaques undergoing active inflammation show

an elevated tCho/tCr ratio, normal or reduced tNAA/tCr ratio (35), and elevated macromolecular signals, possibly arising from myelin breakdown products (114). The tNAA/tCr ratio in the normal-appearing white matter of patients with varying clinical presentations helps differentiate patients from healthy control subjects (115,116) and inversely correlates with disability scores—especially at an early stage (117). In addition, the tCho/tCr ratio is elevated in normal-appearing white matter months before lesions become detectable at conventional MR imaging (118). These observations underscore the ability of MR spectroscopy to characterize white matter abnormality in evolving multiple sclerosis (119). In addition, increasing evidence for gray matter involvement in multiple sclerosis (120) provides motivation to study these lesions with MR spectroscopy as well (113). Finally, MR spectroscopic imaging might play an important role in the differential diagnosis of multiple sclerosis, with acute disseminated encephalomyelitis showing recovery of tNAA signal losses as a favorable prognostic sign (121).

### Focal Lesions Caused by Infectious Agents

Brain infections can be life threatening and, hence, require an early diagnosis for optimal clinical management. Definitive laboratory diagnostic tests can be time consuming, thus delaying therapy. MR spectroscopy is valuable in the differential diagnosis of intracranial ring-enhancing lesions. When a ring-enhancing mass lesion manifests with nonspecific clinical and conventional MR imaging features,  $^1\text{H}$  MR spectroscopy can help confirm the definitive diagnosis of pyogenic abscess and provide information about the type of infective agent (12,122). Demonstration of succinate, acetate, alanine, leucine, isoleucine, and valine are considered specific for pyogenic abscess (Fig 7)—even in the absence of reduced diffusivity at MR imaging. Similarly, parasitic cysts contain succinate and acetate in the absence of amino acids, which helps differentiate them from anaerobic

Figure 6

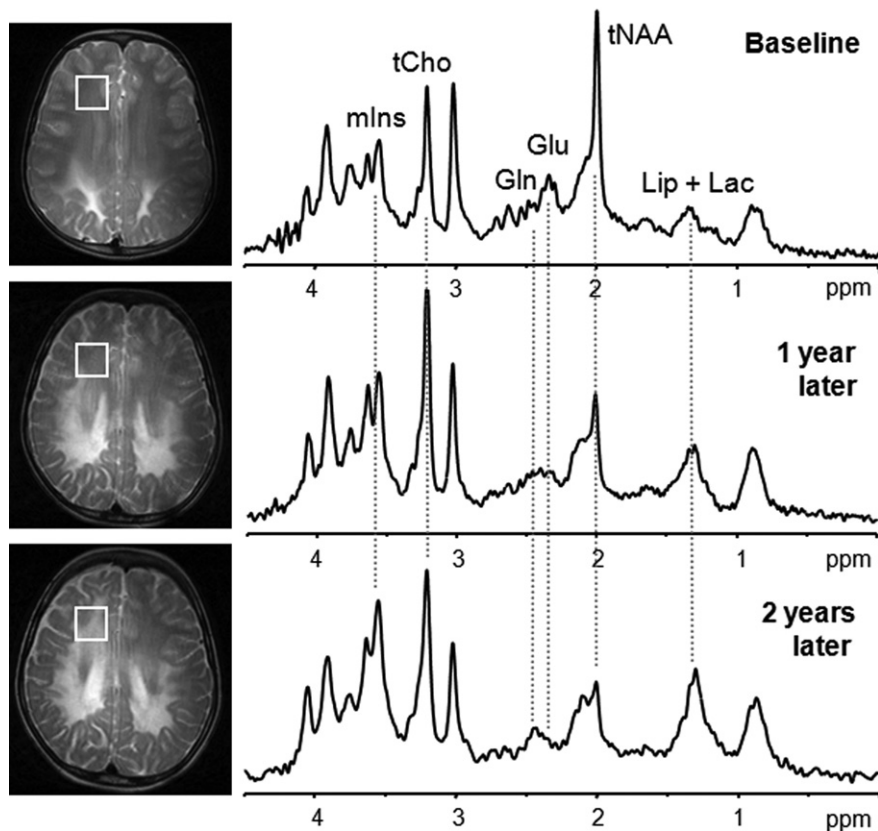


**Figure 6:** Single-voxel  $^1\text{H}$  MR spectroscopy shows progression of disease in boy with X-linked adrenoleukodystrophy. At baseline, T2-weighted signal abnormalities on conventional MR image are seen only in posterior third of centrum semiovale, and spectrum (4.0 T, STEAM, 4500/5, 64 repetitions) is normal. One year later, MR image shows progression of T2 signal abnormalities in middle third of centrum semiovale. Spectrum in anterior third of centrum semiovale already shows increased choline (tCho) and mIns in association with tNAA signal loss. As predicted with the spectrum at 1 year, MR image obtained 2 years later shows further progression of signal changes, with spectrum showing further mIns signal increase and tNAA loss. Also note progressive changes in Glu/Gln ratio and accumulation of mobile lipids (*Lip*) plus Lac at 1- and 2-year follow-up.

abscesses (122,123). MR spectroscopy helps in the differentiation of tuberculoma with solid caseation from other nontuberculous lesions that have a similar appearance at conventional MR imaging. In vivo  $^1\text{H}$  MR spectroscopy from tuberculous abscess shows only Lac and lipid signals and is devoid of cytosolic amino acids. Magnetization transfer ratio MR imaging and amino acid signals in  $^1\text{H}$  MR spectroscopy help differentiate pyogenic from tuberculous abscess (12). MR spectroscopy therefore plays a role in the diagnosis and clinical management of focal brain infections.

### Neurologic Diseases in Which $^1\text{H}$ MR Spectroscopy May Contribute to Patient Management

#### Neurodegenerative Diseases

Neurodegenerative diseases such as Alzheimer disease, Parkinson disease, Huntington disease, amyotrophic lateral sclerosis, and spinocerebellar ataxias are debilitating conditions that result in progressive neuronal degeneration and death. The characteristic feature of neurodegenerative diseases at  $^1\text{H}$  MR spectroscopy is a decrease in tNAA,

typically localized to the region(s) affected by the degenerative process (124,125). The tNAA levels reflect pathologic severity (33,126) (Fig 8) and correlate with clinical measures in cross-sectional studies (127,128). Consistently, tNAA/tCr tends to be lower in subjects with mild cognitive impairment who convert to dementia compared with those who remain stable (129). Therefore, the tNAA/tCr ratio or tNAA concentration may be a valuable prognostic indicator of disease progression, either alone or in combination with volumetric measurements (130).

Other  $^1\text{H}$  MR spectroscopy changes associated with neurodegeneration include a decreased Glu level (128,131,132), an elevated tCho level (125), and an elevated mIns level (132,133). The elevation in mIns may be associated with glial or microglial activation, a characteristic feature of these diseases (134). An elevated mIns level appears early in dementia, preceding the decrease in tNAA concentration (Fig 8), atrophy, and associated neuronal loss and cognitive impairment, as demonstrated in presymptomatic carriers for familial Alzheimer disease (135) and in patients with frontotemporal lobar degeneration mutations (136).

$^1\text{H}$  MR spectroscopy may also be used to monitor treatment response in neurodegenerative diseases. For example, a transient increase in tNAA concentration was associated with short-term functional response during donepezil treatment in Alzheimer disease, suggesting that tNAA also reflects functional integrity and recovery (137). Other studies have shown a decreased mIns/tCr ratio following donepezil treatment (138) and an increased Glu level after galantamine treatment for Alzheimer disease (139).

#### Epilepsy

Epilepsy is a common disorder, with a prevalence of 0.5%–1.0% worldwide. The specific etiology underlying the seizures can be variable, with 60%–70% of all patients responding to medications (140,141). Surgical intervention can be effective in the remaining 30%–40% of

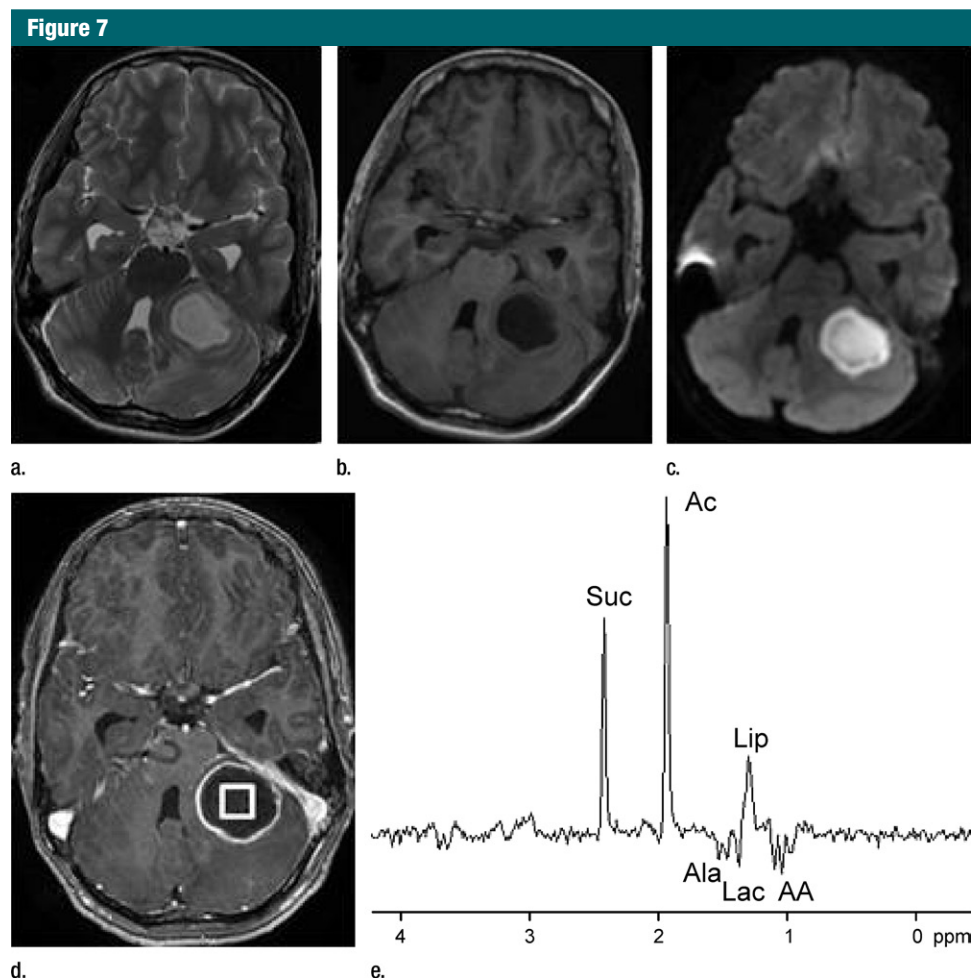


**Figure 7:**  $^1\text{H}$  MR spectroscopy of pyogenic abscess in cerebellum. **(a)** Axial T2-weighted image shows well-defined hyperintense lesion with hypointense wall. **(b)** Axial T1-weighted image shows hypointense lesion with isointense wall. **(c)** Diffusion-weighted image shows restricted diffusion in lesion. **(d)** Postcontrast T1-weighted image shows ring enhancement. **(e)** In vivo  $^1\text{H}$ -MR spectrum (3.0 T, PRESS, 3000/144, 128 repetitions) from center of lesion shows resonances of amino acids (AA, 0.9 ppm), lipid (Lip) and Lac (1.3 ppm), alanine (Ala, 1.5 ppm), acetate (Ac, 1.9 ppm), and succinate (Suc, 2.4 ppm). The resonances from alanine, Lac, and amino acids are inverted at the TE used owing to J evolution.

patients (142,143). In the more common type of focal epilepsy, surgical outcomes are improved if the region of seizure onset can be clearly defined (142,143). Conventional MR imaging can accurately localize the seizure onset region, for example, by identifying unilateral hippocampal atrophy or malformations of cortical development. However, MR imaging may often be negative or ambiguous (eg, bilateral involvement) and, in some cases, lesions seen at MR imaging may not match the focus of seizure onset identified by

means of invasive electroencephalographic measurements.

Given the close physiologic relationship between brain function and metabolism (144), MR spectroscopy has been extensively used to better understand and localize human epilepsy (145,146). Abnormalities in tNAA concentration and the tNAA/tCr ratio have been useful for detecting injured brain in the seizure onset focus (145–149). MR spectroscopic imaging measures have also been extended to neurotransmitters, for example, to assess  $\gamma$ -aminobutyric

acid in patients with epilepsy at ultra-high field strengths (150).

The most common abnormality in temporal lobe epilepsy is mesial temporal sclerosis, which may often be effectively treated with unilateral temporal lobectomy. Multimodal evaluation, which involves scalp or intracranial electroencephalography, conventional MR imaging, and/or metabolic imaging with PET, is commonly used to lateralize the epileptogenic zone in mesial temporal sclerosis. A meta-analysis of  $^1\text{H}$  MR spectroscopy literature comprising 22 studies

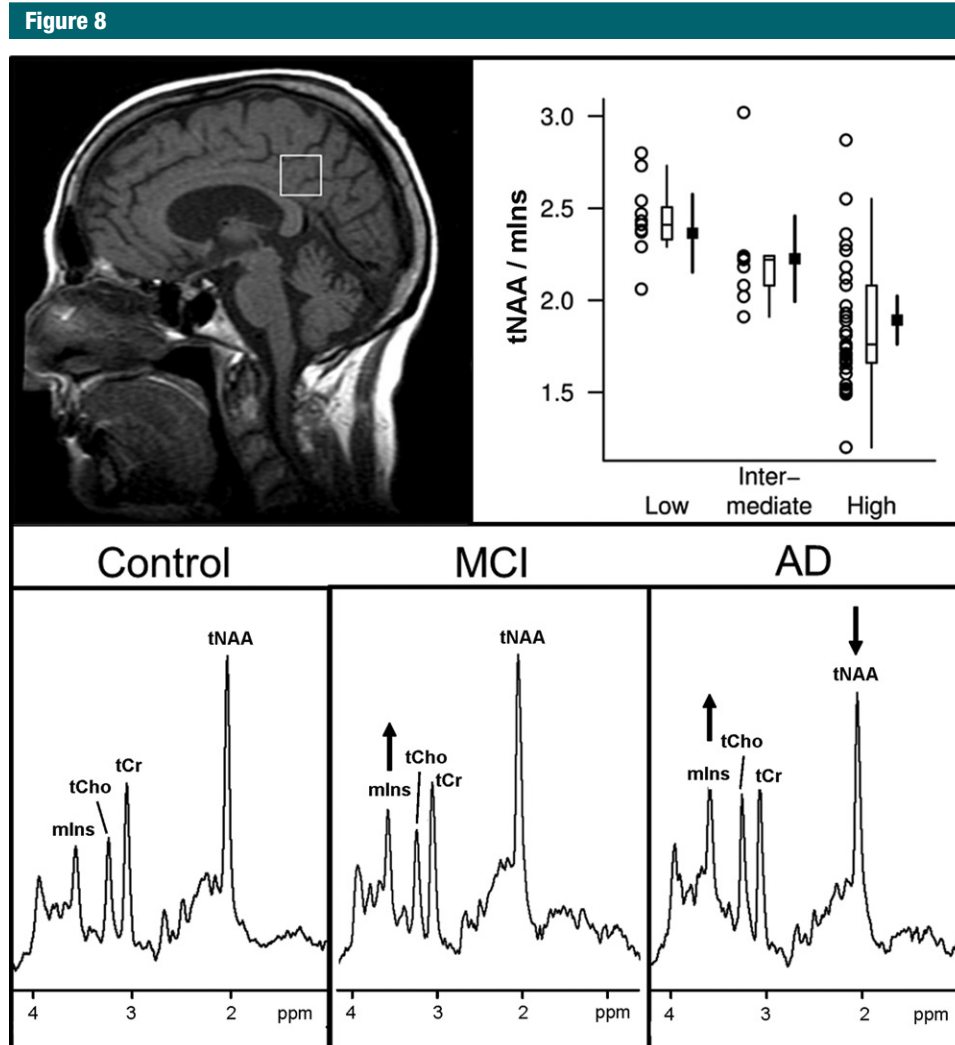


**Figure 8:**  $^1\text{H}$  MR spectroscopic findings at different pathologic and clinical stages of Alzheimer disease. Top panel: Antemortem  $^1\text{H}$  MR spectroscopic findings in posterior cingulate gyrus voxel (T1-weighted midsagittal image) are associated with postmortem pathologic diagnosis of Alzheimer disease (low, intermediate, and high likelihood). For each pathologic diagnosis, plot shows individual values, a box plot of the distribution, and estimated mean and 95% confidence interval for the mean. A strong association is observed with tNAA/mlns ratio ( $R^2 = 0.40$ ;  $P < .001$ ). (Reprinted, with permission, from reference 33.) Bottom panel: Examples of  $^1\text{H}$  MR spectra (1.5 T, PRESS, 2000/30, 128 repetitions) in patients with mild cognitive impairment (MCI) and Alzheimer disease (AD) are compared with that from a cognitively normal subject (control). mlns is elevated as an early marker of subsequent neurodegenerative changes in patient with mild cognitive impairment. tNAA is decreased and mlns is further elevated in patient with Alzheimer disease.

(19 performed with 1.5-T units) indicates that ipsilateral MR spectroscopy abnormality is associated with good outcome following surgery (151). Decreased tNAA/tCr and/or tNAA/(tCr + tCho) ratios were the most common MR spectroscopy indexes for epileptogenic zone. MR spectroscopy may offer potential in presurgical decision making in patients

with no abnormality at conventional MR imaging or in those with a bilateral epileptogenic zone on electroencephalographic recordings. However, MR spectroscopy is still considered a research tool in the context of surgical planning for epilepsy (151). This picture may change when 3.0-T (152) or higher field MR systems (153) are more widely used. MR spectroscopy

may also have value for the assessment of epilepsy in children, with a low tNAA concentration serving as an important index of disease state (154).

#### Acute Stroke and Brain Ischemia

Overall, MR imaging plays a limited role in decision making for clinical management of patients with acute stroke,

Table 2

**Guidelines for Choosing Single- or Multivoxel MR Spectroscopy (MR Spectroscopic Imaging)**

Technique	When to Choose Technique	Advantages	Disadvantages
Single-voxel spectroscopy	Single focal lesion or diffuse disease; to answer a single question (eg, tumor vs abscess); complement to MR spectroscopic imaging in focal lesion (eg, short TE single-voxel spectroscopy to complement long TE MR spectroscopic imaging); in areas of interest close to skull or difficult to obtain an acceptable shim	Acquisition parameters optimized for volume of interest result in high data quality; fast (~2–5 min) if large voxel size (eg, 6–8 mL) is chosen; automatic water reference acquisition standard on most clinical units; data acquisition can be aborted and limited dataset can usually still be used; voxel boundaries generally better defined than with MR spectroscopic imaging	Selected volume is large and block shaped; region of interest must be placed accurately at time of investigation; no information on spatial heterogeneity of lesion and “normal” brain regions; time consuming if multiple locations are to be measured
MR spectroscopic imaging	Undefined, multiple, or heterogeneous lesions; comparison of brain regions in time-efficient manner; diffuse disease (if reliable short TE MR spectroscopic imaging with quantification is available)	Information on tissue heterogeneity; data format compatible with conventional MR imaging (spectroscopic image display integrates with other imaging modalities); larger anatomic coverage; smaller voxel volumes (~1 mL and below) are typically used to assess metabolite distributions; retrospective selection of region of interest within the investigated volume	More exacting system criteria necessary to minimize spectral loss due to insufficient lipid and water suppression (shim over large volumes worse than in single-voxel spectroscopy); longer acquisition times when using conventional encoding (~6–30 min depending on resolution); water reference for quantification adds substantial acquisition time; more experience is needed to plan MR spectroscopic imaging

usually because of a lack of immediate availability of the imaging unit and of patient-related MR imaging safety information. The decision to thrombolysate or to apply any other form of therapeutic intervention in the hyperacute phase is based on clinical grounds and exclusively involves computed tomography to rule out either brain hemorrhage or very large ischemic lesions, which usually have unfavorable outcomes (155). Diffusion-weighted and perfusion MR imaging are superior imaging techniques for detecting acute ischemia and highlight the penumbra, but they are rarely used outside of specialized acute stroke clinics that have rapid access to MR imaging. Similarly,  $^1\text{H}$  MR spectroscopy offers great potential after the hyperacute phase of stroke (beyond 4.5 hours) to assess several key characteristics of ischemic brain for prognostic purposes, such as severity of ischemia and neuronal dysfunction and damage.

Preclinical work has shown that tNAA decreases in ischemic brain parenchyma in a linear fashion for the first 6 hours, followed by a slower decrease for the subsequent 24 hours (156,157).

The concentration of tNAA in brain parenchyma after ischemia (158) and in chronic infarction may even decrease below the level of detection with *in vivo*  $^1\text{H}$  MR spectroscopy (4). Measurement of tNAA levels could influence patient management; severely decreased tNAA appears to be related to clinical stroke syndrome and more extensive infarction, both indexes of poor clinical outcome (36). A decrease in tNAA on follow-up MR spectroscopy data has been associated with ongoing ischemia and progressing infarction (159).

Lac is another metabolite with potential value for clinical evaluation in stroke. Lac is the end product of non-oxidative glucose consumption and is commonly considered as a signature of hypoxia and/or ischemia. Elevated Lac in the core of ischemic tissue correlates with final infarct size and clinical outcome (159). The presence of Lac with a concomitant reduction in tNAA was observed in large infarcts with poor outcome (36). Lac levels that are persistently elevated for weeks in infarcted brain parenchyma have been associated with inflammatory macrophages (160).

Therefore, quantitative metabolite data for tNAA and Lac are of value for evaluating the nature of ischemia and predicting risk for new ischemic events (161).

### Technical Considerations

#### Data Acquisition

Any application of MR spectroscopy to a clinical question starts with the decision about a pulse sequence and parameters. In general, this choice is dictated by the disease (Table 2). When the affected brain region is well defined, single-voxel spectroscopy is the preferred method and provides robust metabolite quantification in the selected volume of interest, whereas MR spectroscopic imaging is the method of choice in diseases where the focal point of pathology is unclear, if there are multiple lesions, or if the lesions are heterogeneous. For example, MR spectroscopic imaging is advantageous in the accurate evaluation of tissue status in localization-related epilepsy (Table 1) and in the investigation of the heterogeneity of large tumors (67). In

**Figure 9**

✓ SNR > 3 for major resonances such as high tCho and low tNAA in tumors; SNR > 2 for detection only of important indicator metabolites such as lactate
✓ Spectral resolution: FWHM of metabolites < 0.1 ppm
✓ Line shape: symmetric
✓ Water suppression > 98%
✓ No lipid contamination from the scalp
✓ Artifacts (chemical shift artifact, ghosting, patient motion, eddy currents, volume averaging) are absent or minor

**Figure 9:** Minimum technical requirements to ensure that a  $^1\text{H}$  MR spectrum is clinically interpretable. SNR is calculated from a nonapodized spectrum by using maximum height of largest signal (typically tNAA) divided by standard deviation of noise. Note that these SNR limits are given only for visual assessment of spectra for ratio changes in major metabolites or for presence or absence of metabolites such as Lac. Higher SNR levels are necessary for reliable quantification of metabolites. *FWHM* = full width at half maximum.

many abnormalities, single-voxel spectroscopy and MR spectroscopic imaging can be used in combination; for example, MR spectroscopic imaging to first identify the lesion location and single-voxel spectroscopy to quantify metabolites that can be reliably obtained from high-quality, short TE spectra in the identified lesion (Table 1).

All of the major clinical MR imaging vendors provide MR spectroscopy protocols, primarily with use of the basic PRESS (1,2) and STEAM (3) sequences (Table 1). In addition, other state-of-the-art single-voxel spectroscopy and MR spectroscopic imaging sequences, which offer various advantages over the basic STEAM and PRESS sequences, have been implemented on some clinical platforms (Appendix E1 [online]).

Which field strength is optimal for a particular clinical application of MR spectroscopy is another important question for the practicing neuroradiologist and clinical trialist. Although 3.0 T is becoming the preferred platform over 1.5-T for MR spectroscopy owing to

potential gains in SNR and spectral resolution, it is important to note that field strength is not the sole determinant of the information content of spectra. In fact, a spectrum obtained at 1.5 T with a protocol adhering to spectral quality standards (Appendix E1 [online], Fig 9) provides more reliable metabolite information than a poor-quality spectrum obtained at 3.0 T. Overall, clinical MR spectroscopy can be successfully performed at either 1.5 or 3.0 T for the majority of applications. Although the potential gains at magnetic fields higher than 3.0 T for clinical MR spectroscopy are still being assessed, significant improvements in spectral and spatial resolution at 7.0 T have been reported. For example, previously inaccessible alterations in low-concentration metabolites may be uncovered at 7.0 T (162). For MR spectroscopic imaging, the nominal spatial resolution can be reduced to 0.14 mL at 7.0 T (163).

Finally, the importance of spectral quality generated with the chosen pulse sequence, parameters, and field strength cannot be underestimated. For reliable clinical decision making based on MR spectroscopy data, obtaining high-quality, artifact-free spectra is crucial. The sources and forms of artifacts in MR spectra have been reviewed in detail (164) and are summarized in Appendix E1 (online). The detection of such artifacts and exclusion of spectra based on predefined quality criteria relies on the human expert in most applications of single-voxel spectroscopy, whereas automated quality assessment of MR spectroscopic imaging data is preferred. A practical guide to determine whether a spectrum is adequate for clinical use is provided in Figure 9. Further considerations regarding the choices for clinical MR spectroscopy data acquisition, including pulse sequence, parameters, field strength, and radiofrequency coils, as well as recommendations for spectral quality assessments, are detailed in Appendix E1 (online).

### Data Analysis and Reporting

All clinical imaging units provide MR spectroscopy analysis software, which

can be used for visual inspection of spectra and basic quantification of metabolite ratios. In addition, off-line postprocessing tools (165) and sophisticated quantification packages such as LCModel (166) are widely used. These packages provide quantitative error estimates for metabolite quantification (eg, Cramér-Rao lower bounds), with which the reliability of metabolite concentrations can be assessed (see Appendix E1 [online] for recommended criteria). The availability of error estimates is an important requirement for clinical decision making when using quantitative MR spectroscopy measures; therefore, vendors of clinical imaging units are encouraged to implement more robust, U.S. Food and Drug Administration–approved MR spectroscopy analysis packages that provide such quantitative error estimates.

For clinical use, single-voxel spectroscopy data can be reported numerically as metabolite concentrations or as ratios, ideally supplemented with visualization of volume of interest placement (167). On the other hand, information from two- or three-dimensional MR spectroscopic imaging must be made available to the clinician in a quick and easy image format to incorporate into the clinical routine. In addition, implementation of MR spectroscopy into picture archiving and communication systems is recommended to facilitate easy access to MR spectroscopy data in the standard work environment.

### Reproducibility and Clinical Translation

Ultimately, test-retest reproducibility of measured metabolite levels determines the utility of MR spectroscopy for disease assessment. To be of clinical value, experimental and biologic variability in the quantified metabolite levels must be smaller than their changes caused by disease. Test-retest coefficients of variance reported at 1.5 and 3.0 T (168–173) show improved accuracy for several metabolites at higher fields and shorter TEs. Test-retest coefficients of variance of 6% or less are achievable for five metabolites (tNAA, tCr, tCho, mIns, Glu) with single-voxel

Figure 10

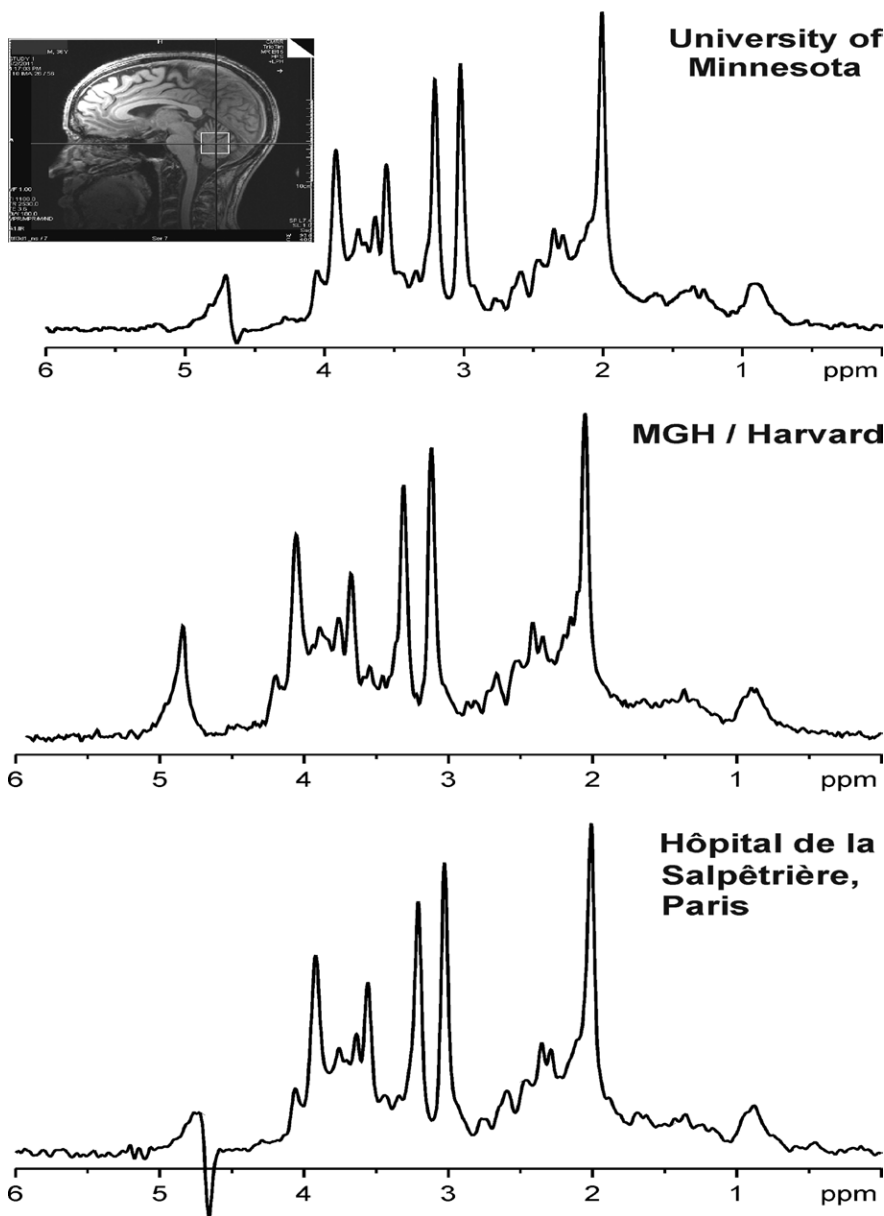


**Figure 10:** Comparison of MR spectral quality at multiple sites.  $^1\text{H}$  MR spectra were acquired at three different sites from cerebellar volume of interest ( $10 \times 25 \times 25 \text{ mm}^3$ , as shown on T1-weighted midsagittal image) in three healthy individuals. Spectra were obtained with 3.0-T MR unit (Tim Trio; Siemens Healthcare, Erlangen, Germany) with same acquisition protocol (fast automatic shimming technique by mapping along projections, or FASTMAP, semi-LASER [localization by adiabatic selective refocusing] [175], 5000/28, 64 repetitions). (Spectrum from Hôpital de la Salpêtrière courtesy of Fanny Mochel, MD, PhD.) MGH = Massachusetts General Hospital.

spectroscopy at 3.0 T (174), and coefficients of variance less than 10% were reported for tNAA, tCr, tCho, and mIns with MR spectroscopic imaging at 3.0 T

(172,173). Importantly, standard clinical hardware generates reproducible MR spectroscopy data from the human brain in a multicenter setting provided

that identical and optimized acquisition protocols and calibration schemes are used (Fig 10).

When it is desired to use clinical MR spectroscopy data to make decisions affecting management, it is essential that an adequate cohort of subjects has been studied such that the classifier used is robust in terms of both sensitivity and specificity. Recommended cohort size will depend somewhat on the nature of the data, but anything less than several hundred subjects, both healthy subjects and those with the condition of interest, would not yield a classifier that would be certified for use by a regulatory agency. A detailed discussion of these issues has appeared recently (176,177).

In addition, validation of MR spectroscopy biomarkers for clinical use requires their incorporation in robust prospective multicenter clinical trials, where patient selection and treatment meets prespecified criteria and the statistical methodology is set before the trial commences. This requires careful MR spectroscopy protocol design that can be adhered to at all the participating centers. In addition, effective, real-time quality control measures must be put in place to ensure that data that need to be discarded are kept to a minimum to avoid bias and ensure generalizability of the results.

Appendix E1 (online) highlights further recommendations to facilitate translation of MR spectroscopy to routine use in the clinical environment, including steps that must be taken for integration with clinical imaging and for quality management in single- and multisite studies (Fig 10) and a discussion on reimbursement issues, a frequently cited impediment to the widespread use of clinical MR spectroscopy.

### Conclusions and Recommendations

In conclusion, MR spectroscopy is used worldwide as an adjunct to MR imaging in several common neurologic diseases, including brain neoplasms, inherited metabolic disorders, demyelinating disorders, and infective focal lesions. The spectrum of disorders for which

MR spectroscopy will be clinically used is likely to expand; potential examples include neurodegenerative diseases and epilepsy. The standardization of MR spectroscopy data acquisition and analysis techniques for clinical use is encouraged, along with the publication of normative data obtained with these techniques. Multicenter trials are encouraged to establish the utility of MR spectroscopy in large enough sample sizes to definitively establish the value of MR spectroscopy in specific clinical applications. Where possible, these should include assessment of the impact on clinical outcome and economic benefit. Clinical imaging centers specializing in combined use of MR imaging and spectroscopy should be established in all major clinical neurologic centers that offer standardized MR spectroscopy procedures for improved patient management. Manufacturers of MR units and third-party companies (eg, vendors of analysis software) are encouraged to continue to develop their products to incorporate recent technical advances, to obtain U.S. Food and Drug Administration approval for clinical use, and to provide products with manufacturer-independent standardized outputs.

**Acknowledgments:** The initiative for the MRS Consensus paper was proposed by Risto Kauppinen, MD, PhD, in the MR spectroscopy session of the 8th Biennial Minnesota Workshop on High and Ultra-high Field Imaging held in Minneapolis, Minn, in October 2011. Drs Kauppinen and Öz invited the expert contributors to the paper in due course and organized teleconferences and special interest group meetings held in connection to the International Society for Magnetic Resonance in Medicine (ISMRM) conferences to coordinate the preparation of the manuscript. A subcommittee formed by Jens Frahm, PhD, Roland Kreis, PhD, Peter Barker, DPhil, Andrew Peet, MD, PhD, and Alberto Bizzi, MD, played a major role in editing drafts of the manuscript. The contributors would like to thank Philips Healthcare for making the first special interest group session at ISMRM possible.

**Complete list of authors (listed in alphabetic order except for first and last authors):** Gülin Öz, PhD; Jeffrey R. Alger, MPhil, PhD; Peter B. Barker, DPhil; Robert Bartha, PhD; Alberto Bizzi, MD; Chris Boesch, MD, PhD; Patrick J. Bolan, PhD; Kevin M. Brindle, DPhil; Cristina Cudalbu, PhD; Alp Dinçer, MD; Ulrike Dydak, PhD; Uzay E. Emir, PhD; Jens Frahm, PhD;

Ramón Gilberto González, MD, PhD; Stephan Gruber, PhD; Rolf Gruetter, PhD; Rakesh K. Gupta, MD; Arend Heerschap, PhD; Anke Henning, PhD; Hoby P. Hetherington, PhD; Franklyn A. Howe, DPhil; Petra S. Hüppi, MD; Ralph E. Hurd, PhD; Kejal Kantarci, MD; Dennis W. J. Klomp, PhD; Roland Kreis, PhD; Marijn J. Kruskamp, PhD; Martin O. Leach, PhD; Alexander P. Lin, PhD; Peter R. Luijten, PhD; Małgorzata Marjańska, PhD; Andrew A. Maudsley, PhD; Dieter J. Meyerhoff, Dr rer nat; Carolyn E. Mountford, DPhil; Sarah J. Nelson, PhD; M. Necmettin Pamir, MD; Jullie W. Pan, MD, PhD; Andrew C. Peet, MD, PhD; Harish Poptani, PhD; Stefan Posse, PhD; Petra J. W. Pouwels, PhD; Eva-Maria Ratai, PhD; Brian D. Ross, MD; Tom W. J. Scheenen, PhD; Christian Schuster, PhD; Ian C. P. Smith, OC, PhD, DSc; Brian J. Soher, PhD; Ivan Tkáč, PhD; Daniel B. Vigneron, PhD; and Risto A. Kauppinen, MD, PhD.

**Author affiliations:** Center for Magnetic Resonance Research, University of Minnesota, 2021 6th St SE, Minneapolis, MN 55455 (G.O., P.J.B., M.M., I.T.); Department of Radiology, University of California–Los Angeles, Los Angeles, Calif (J.R.A.); Department of Radiology, Johns Hopkins University School of Medicine, Baltimore, Md (P.B.B.); Roberts Research Institute, University of Western Ontario, London, Ont, Canada (R.B.); Neuroradiology Unit, Istituto Clinico Humanitas IRCCS, Milan, Italy (A.B.); Departments of Radiology and Clinical Research, University of Bern, Bern, Switzerland (C.B., R.K.); Department of Biochemistry, University of Cambridge, Cambridge, England (K.M.B.); Laboratory for Functional and Metabolic Imaging (LIFMET), Center for Biomedical Imaging (CIBM), Ecole Polytechnique Fédérale de Lausanne (EPFL), Lausanne, Switzerland (C.C., R.G.); Acibadem University, School of Medicine, Istanbul, Turkey (A.D., M.N.P.); School of Health Sciences, Purdue University, West Lafayette, Ind (U.D.); Oxford Centre for Functional MRI of the Brain (FMRIB), John Radcliffe Hospital, Headington, Oxford, England (U.E.E.); Biomedizinische NMR Forschungs GmbH am Max-Planck-Institut für biophysikalische Chemie, Göttingen, Germany (J.F.); Department of Radiology, Massachusetts General Hospital, Harvard University, Boston, Mass (R.G.G., E.M.R.); Department of Radiology, Medical University of Vienna, Vienna, Austria (S.G.); Department of Radiology, Sanjay Gandhi Post Graduate Institute of Medical Sciences, Lucknow, India (R.K.G.); Department of Radiology, Radboud University Nijmegen Medical Center, Nijmegen, the Netherlands (A. Heerschap, T.W.J.S.); Max Planck Institute of Biological Cybernetics, Tübingen, Germany and Institute for Biomedical Engineering, University and ETH Zurich, Zurich, Switzerland (A. Henning); Department of Radiology, University of Pittsburgh, Pittsburgh, Pa (H.P.H.); Clinical Sciences, St George's, University of London, London, England (F.A.H.); Department of Pediatrics, University of Geneva, Geneva, Switzerland (P.S.H.); General Electric Healthcare, Menlo Park, Calif (R.E.H.); Department of Radiology, Mayo Clinic, Rochester, Minn (K.K.); University Med-

ical Centre Utrecht, Utrecht, the Netherlands (D.W.J.K., P.R.L.); Philips Healthcare, Best, the Netherlands (M.J.K.); CR-UK and EPSRC Cancer Imaging Centre, Institute of Cancer Research, University of London, Sutton, England (M.O.L.); Centre for MR in Health, Centre for Clinical Spectroscopy, Brigham and Women's Hospital, Harvard University Medical School, Boston, Mass (A.P.L., C.E.M.); Department of Radiology, University of Miami, Miami, Fla (A.A.M.); DVA Medical Center and Department of Radiology and Biomedical Imaging, University of California San Francisco, San Francisco, Calif (D.J.M.); Centre for MR in Health, University of Newcastle, Newcastle, Australia (C.E.M.); Department of Radiology and Biomedical Imaging, University of California San Francisco, San Francisco, Calif (S.J.N., D.B.V.); Department of Neurology, University of Pittsburgh, Pittsburgh, Pa (J.W.P.); Department of Cancer Sciences, University of Birmingham, Birmingham, England (A.C.P.); Department of Radiology, University of Pennsylvania, Philadelphia, Pa (H.P.); Department of Neurology, University of New Mexico, Albuquerque, NM (S.P.); VU University Medical Center Amsterdam, Amsterdam, the Netherlands (P.J.W.P.); Huntington Medical Research Center, Pasadena, Calif (B.D.R.); Siemens Healthcare, Erlangen, Germany (C.S.); Innovative Biodiagnostics, Winnipeg, Canada (I.C.P.S.); Department of Radiology, Duke University Medical Center, Durham, NC (B.J.S.); and School of Experimental Psychology and Clinical Research and Imaging Centre, University of Bristol, Bristol, England (R.A.K.)

**Disclosures of Conflicts of Interest:** **G.O.** No relevant conflicts of interest to disclose. **J.R.A.** No relevant conflicts of interest to disclose. **P.B.B.** Financial activities related to the present article: is a consultant for Olea Medical. Financial activities not related to the present article: none to disclose. Other relationships: none to disclose. **R.B.** Financial activities related to the present article: none to disclose. Financial activities not related to the present article: receives personal fees from Bioscope Imaging Solutions. Other relationships: none to disclose. **A.B.** No relevant conflicts of interest to disclose. **C.B.** No relevant conflicts of interest to disclose. **P.J.B.** No relevant conflicts of interest to disclose. **K.M.B.** No relevant conflicts of interest to disclose. **C.C.** No relevant conflicts of interest to disclose. **A.D.** No relevant conflicts of interest to disclose. **U.D.** Financial activities related to the present article: none to disclose. Financial activities not related to the present article: receives payment for board membership from GyroTools. Other relationships: none to disclose. **U.E.E.** No relevant conflicts of interest to disclose. **J.F.** No relevant conflicts of interest to disclose. **R.G.G.** No relevant conflicts of interest to disclose. **S.G.** No relevant conflicts of interest to disclose. **R.G.** No relevant conflicts of interest to disclose. **R.K.G.** No relevant conflicts of interest to disclose. **A. Heerschap** No relevant conflicts of interest to disclose. **A. Henning** No relevant conflicts of interest to disclose. **H.P.H.** No relevant conflicts of interest to disclose. **F.A.H.** Financial activities related to the present article: none to disclose. Financial activities not related to the

present article: has a patent pending. Other relationships: none to disclose. **P.S.H.** No relevant conflicts of interest to disclose. **R.E.H.** Financial activities related to the present article: none to disclose. Financial activities not related to the present article: is employed by GE Healthcare. Other relationships: none to disclose. **K.K.** Financial activities related to the present article: institution received fees for participation in review activities such as data monitoring boards, statistical analysis, end point committees and the like from Takeda Global Research, Pfizer, and Janssen Alzheimer's Immunotherapy. Financial activities not related to the present article: institution receives payment for board membership from Takeda Global Research, Pfizer, and Janssen Alzheimer's Immunotherapy. Other relationships: none to disclose. **D.W.J.K.** No relevant conflicts of interest to disclose. **R.K.** No relevant conflicts of interest to disclose. **M.J.K.** Financial activities related to the present article: none to disclose. Financial activities not related to the present article: is employed by Philip Healthcare. Other relationships: none to disclose. **M.O.L.** Financial activities related to the present article: none to disclose. Financial activities not related to the present article: receives nonfinancial support from Siemens, Philips, and GE; received a grant from Philips. Other relationships: none to disclose. **A.P.L.** No relevant conflicts of interest to disclose. **P.R.L.** No relevant conflicts of interest to disclose. **M.M.** No relevant conflicts of interest to disclose. **A.A.M.** No relevant conflicts of interest to disclose. **D.J.M.** No relevant conflicts of interest to disclose. **C.E.M.** Financial activities related to the present article: none to disclose. Financial activities not related to the present article: none to disclose. Other relationships: has a patent with Innovative Biodiagnostics. **S.J.N.** No relevant conflicts of interest to disclose. **M.N.P.** No relevant conflicts of interest to disclose. **J.W.P.** No relevant conflicts of interest to disclose. **A.C.P.** Financial activities related to the present article: none to disclose. Financial activities not related to the present article: institution has grants/grants pending with Action Medical Research. Other relationships: none to disclose. **H.P.** No relevant conflicts of interest to disclose. **S.P.** Financial activities related to the present article: none to disclose. Financial activities not related to the present article: none to disclose. Other relationships: has patents. **P.J.W.P.** No relevant conflicts of interest to disclose. **E.M.R.** No relevant conflicts of interest to disclose. **B.D.R.** No relevant conflicts of interest to disclose. **T.W.J.S.** Financial activities related to the present article: none to disclose. Financial activities not related to the present article: has a grant with Siemens Healthcare. Other relationships: none to disclose. **C.S.** Financial activities related to the present article: none to disclose. Financial activities not related to the present article: is employed by Siemens Healthcare. Other relationships: none to disclose. **I.C.P.S.** No relevant conflicts of interest to disclose. **B.J.S.** No relevant conflicts of interest to disclose. **I.T.** No relevant conflicts of interest to disclose. **D.B.V.** No relevant conflicts of interest to disclose. **R.A.K.** No relevant conflicts of interest to disclose.

## References

- Bottomley PA. Selective volume method for performing localized NMR spectroscopy. U.S. patent 4,480,228. 1984.
- Ordidge RJ, Bendall MR, Gordon RE, Connelly A. Volume selection for in vivo biological spectroscopy. In: Govil G, Khatri CL, Saran A, eds. *Magnetic resonance in biology and medicine*. New Delhi, India: McGraw Hill, 1985; 387–397.
- Frahm J, Merboldt KD, Hänicke W. Localized proton spectroscopy using stimulated echoes. *J Magn Reson* 1987;72(3):502–508.
- Bruhn H, Frahm J, Gyngell ML, Merboldt KD, Hänicke W, Sauter R. Cerebral metabolism in man after acute stroke: new observations using localized proton NMR spectroscopy. *Magn Reson Med* 1989;9(1):126–131.
- Arnold DL, Matthews PM, Francis G, Antel J. Proton magnetic resonance spectroscopy of human brain in vivo in the evaluation of multiple sclerosis: assessment of the load of disease. *Magn Reson Med* 1990;14(1):154–159.
- Bruhn H, Frahm J, Gyngell ML, et al. Non-invasive differentiation of tumors with use of localized H-1 MR spectroscopy in vivo: initial experience in patients with cerebral tumors. *Radiology* 1989;172(2):541–548.
- Bottomley PA. The trouble with spectroscopy papers. *Radiology* 1991;181(2):344–350.
- Lin AP, Tran TT, Ross BD. Impact of evidence-based medicine on magnetic resonance spectroscopy. *NMR Biomed* 2006;19(4):476–483.
- Fryback DG, Thornbury JR. The efficacy of diagnostic imaging. *Med Decis Making* 1991;11(2):88–94.
- Govindaraju V, Young K, Maudsley AA. Proton NMR chemical shifts and coupling constants for brain metabolites. *NMR Biomed* 2000;13(3):129–153.
- De Graaf RA. *In vivo NMR spectroscopy: principles and techniques*. 2nd ed. Hoboken, NJ: Wiley, 2007.
- Gupta RK. Magnetic resonance spectroscopy in intracranial infection. In: Gillard JH, Waldman AD, Barker PB, eds. *Clinical MR neuroimaging*. 2nd ed. London, England: Cambridge University Press, 2010; 426–454.
- Howe FA, Barton SJ, Cudlip SA, et al. Metabolic profiles of human brain tumors using quantitative in vivo <sup>1</sup>H magnetic resonance spectroscopy. *Magn Reson Med* 2003;49(2):223–232.
- Öz G, Tkáč I, Charnas LR, et al. Assessment of adrenoleukodystrophy lesions by high field MRS in non-sedated pediatric patients. *Neurology* 2005;64(3):434–441.
- Oakden WK, Noseworthy MD. Propylene glycol is essential in the LCModel basis set for pediatric <sup>1</sup>H-MRS. *J Comput Assist Tomogr* 2005;29(1):136–139.
- Fein G, Meyerhoff DJ. Ethanol in human brain by magnetic resonance spectroscopy: correlation with blood and breath levels, relaxation, and magnetization transfer. *Alcohol Clin Exp Res* 2000;24(8):1227–1235.
- Gruetter R, Weisdorf SA, Rajanayagan V, et al. Resolution improvements in in vivo <sup>1</sup>H NMR spectra with increased magnetic field strength. *J Magn Reson* 1998;135(1):260–264.
- Otazo R, Mueller B, Ugurbil K, Wald L, Posse S. Signal-to-noise ratio and spectral linewidth improvements between 1.5 and 7 Tesla in proton echo-planar spectroscopic imaging. *Magn Reson Med* 2006;56(6):1200–1210.
- Frahm J, Bruhn H, Gyngell ML, Merboldt KD, Hänicke W, Sauter R. Localized proton NMR spectroscopy in different regions of the human brain in vivo: relaxation times and concentrations of cerebral metabolites. *Magn Reson Med* 1989;11(1):47–63.
- Mlynárik V, Gruber S, Moser E. Proton T (1) and T (2) relaxation times of human brain metabolites at 3 Tesla. *NMR Biomed* 2001;14(5):325–331.
- Hofmann L, Slotboom J, Jung B, Maloca P, Boesch C, Kreis R. Quantitative <sup>1</sup>H-magnetic resonance spectroscopy of human brain: influence of composition and parameterization of the basis set in linear combination model-fitting. *Magn Reson Med* 2002;48(3):440–453.
- Mekle R, Mlynárik V, Gambarota G, Hergt M, Krueger G, Gruetter R. MR spectroscopy of the human brain with enhanced signal intensity at ultrashort echo times on a clinical platform at 3T and 7T. *Magn Reson Med* 2009;61(6):1279–1285.
- Tkáč I, Öz G, Adriany G, Ugurbil K, Gruetter R. In vivo <sup>1</sup>H NMR spectroscopy of the human brain at high magnetic fields: metabolite quantification at 4T vs. 7T. *Magn Reson Med* 2009;62(4):868–879.
- Deelchand DK, Van de Moortele PF, Adriany G, et al. In vivo <sup>1</sup>H NMR spectroscopy of the human brain at 9.4 T: initial results. *J Magn Reson* 2010;206(1):74–80.
- Marjańska M, Auerbach EJ, Valabrégue R, Van de Moortele PF, Adriany G, Gar-

- wood M. Localized <sup>1</sup>H NMR spectroscopy in different regions of human brain in vivo at 7 T: T2 relaxation times and concentrations of cerebral metabolites. *NMR Biomed* 2012;25(2):332–339.
26. Urenjak J, Williams SR, Gadian DG, Noble M. Specific expression of *N*-acetylaspartate in neurons, oligodendrocyte-type-2 astrocyte progenitors, and immature oligodendrocytes in vitro. *J Neurochem* 1992;59(1):55–61.
27. Tallan HH. Studies on the distribution of *N*-acetyl-L-aspartic acid in brain. *J Biol Chem* 1957;224(1):41–45.
28. Moffett JR, Namboodiri MA, Cangro CB, Neale JH. Immunohistochemical localization of *N*-acetylaspartate in rat brain. *Neuroreport* 1991;2(3):131–134.
29. Miller BL. A review of chemical issues in <sup>1</sup>H NMR spectroscopy: *N*-acetyl-L-aspartate, creatine and choline. *NMR Biomed* 1991;4(2):47–52.
30. Rigotti DJ, Inglese M, Gonen O. Whole-brain *N*-acetylaspartate as a surrogate marker of neuronal damage in diffuse neurologic disorders. *AJNR Am J Neuroradiol* 2007;28(10):1843–1849.
31. Bates TE, Strangward M, Keelan J, Davey GP, Munro PM, Clark JB. Inhibition of *N*-acetylaspartate production: implications for <sup>1</sup>H MRS studies in vivo. *Neuroreport* 1996;7(8):1397–1400.
32. Pouwels PJ, Kruse B, Korenke GC, Mao X, Hanefeld FA, Frahm J. Quantitative proton magnetic resonance spectroscopy of childhood adrenoleukodystrophy. *Neuropediatrics* 1998;29(5):254–264.
33. Kantarci K, Knopman DS, Dickson DW, et al. Alzheimer disease: postmortem neuropathologic correlates of antemortem <sup>1</sup>H MR spectroscopy metabolite measurements. *Radiology* 2008;248(1):210–220.
34. Licata SC, Renshaw PF. Neurochemistry of drug action: insights from proton magnetic resonance spectroscopic imaging and their relevance to addiction. *Ann N Y Acad Sci* 2010;1187:148–171.
35. Richards TL. Proton MR spectroscopy in multiple sclerosis: value in establishing diagnosis, monitoring progression, and evaluating therapy. *AJR Am J Roentgenol* 1991;157(5):1073–1078.
36. Wardlaw JM, Marshall I, Wild J, Dennis MS, Cannon J, Lewis SC. Studies of acute ischemic stroke with proton magnetic resonance spectroscopy: relation between time from onset, neurological deficit, metabolite abnormalities in the infarct, blood flow, and clinical outcome. *Stroke* 1998;29(8):1618–1624.
37. Groenendaal F, Veenhoven RH, van der Grond J, Jansen GH, Witkamp TD, de Vries LS. Cerebral lactate and *N*-acetylaspartate/choline ratios in asphyxiated full-term neonates demonstrated in vivo using proton magnetic resonance spectroscopy. *Pediatr Res* 1994;35(2):148–151.
38. Lange T, Dydak U, Roberts TP, Rowley HA, Bjeljac M, Boesiger P. Pitfalls in lactate measurements at 3T. *AJNR Am J Neuroradiol* 2006;27(4):895–901.
39. Gill SS, Thomas DG, Van Bruggen N, et al. Proton MR spectroscopy of intracranial tumours: in vivo and in vitro studies. *J Comput Assist Tomogr* 1990;14(4):497–504.
40. Peeling J, Sutherland G. High-resolution <sup>1</sup>H NMR spectroscopy studies of extracts of human cerebral neoplasms. *Magn Reson Med* 1992;24(1):123–136.
41. Florian CL, Preece NE, Bhakoo KK, Williams SR, Noble M. Characteristic metabolic profiles revealed by <sup>1</sup>H NMR spectroscopy for three types of human brain and nervous system tumours. *NMR Biomed* 1995;8(6):253–264.
42. Hourani R, Brant LJ, Rizk T, Weingart JD, Barker PB, Horska A. Can proton MR spectroscopic and perfusion imaging differentiate between neoplastic and nonneoplastic brain lesions in adults? *AJNR Am J Neuroradiol* 2008;29(2):366–372.
43. Law M, Yang S, Wang H, et al. Glioma grading: sensitivity, specificity, and predictive values of perfusion MR imaging and proton MR spectroscopic imaging compared with conventional MR imaging. *AJNR Am J Neuroradiol* 2003;24(10):1989–1998.
44. Garca-Gomez JM, Luts J, Julia-Sape M, et al. Multiproject-multicenter evaluation of automatic brain tumor classification by magnetic resonance spectroscopy. *MAGMA* 2009;22(1):5–18.
45. Vicente J, Fuster-Garca E, Tortajada S, et al. Accurate classification of childhood brain tumours by in vivo <sup>1</sup>H MRS: a multi-centre study. *Eur J Cancer* 2013;49(3):658–667.
46. Tate AR, Underwood J, Acosta DM, et al. Development of a decision support system for diagnosis and grading of brain tumours using in vivo magnetic resonance single voxel spectra. *NMR Biomed* 2006;19(4):411–434.
47. Choi C, Ganji SK, DeBerardinis RJ, et al. 2-hydroxyglutarate detection by magnetic resonance spectroscopy in IDH-mutated patients with gliomas. *Nat Med* 2012;18(4):624–629.
48. Julia-Sape M, Coronel I, Majos C, et al. Prospective diagnostic performance evaluation of single-voxel <sup>1</sup>H MRS for typing and grading of brain tumours. *NMR Biomed* 2012;25(4):661–673.
49. Opstad KS, Ladroue C, Bell BA, Griffiths JR, Howe FA. Linear discriminant analysis of brain tumour <sup>1</sup>H MR spectra: a comparison of classification using whole spectra versus metabolite quantification. *NMR Biomed* 2007;20(8):763–770.
50. Crawford FW, Khayal IS, McGue C, et al. Relationship of pre-surgery metabolic and physiological MR imaging parameters to survival for patients with untreated GBM. *J Neurooncol* 2009;91(3):337–351.
51. Murphy PS, Rowland IJ, Viviers L, Brada M, Leach MO, Dzik-Jurasz AS. Could assessment of glioma methylene lipid resonance by in vivo <sup>1</sup>H-MRS be of clinical value? *Br J Radiol* 2003;76(907):459–463.
52. Poptani H, Gupta RK, Roy R, Pandey R, Jain VK, Chhabra DK. Characterization of intracranial mass lesions with in vivo proton MR spectroscopy. *AJNR Am J Neuroradiol* 1995;16(8):1593–1603.
53. Kovanlikaya A, Panigrahy A, Krieger MD, et al. Untreated pediatric primitive neuroectodermal tumor in vivo: quantitation of taurine with MR spectroscopy. *Radiology* 2005;236(3):1020–1025.
54. Davies NP, Wilson M, Natarajan K, et al. Non-invasive detection of glycine as a biomarker of malignancy in childhood brain tumours using in-vivo <sup>1</sup>H MRS at 1.5 Tesla confirmed by ex-vivo high-resolution magic-angle spinning NMR. *NMR Biomed* 2010;23(1):80–87.
55. McKnight TR, Lamborn KR, Love TD, et al. Correlation of magnetic resonance spectroscopic and growth characteristics within grades II and III gliomas. *J Neurosurg* 2007;106(4):660–666.
56. Chang SM, Nelson S, Vandenberg S, et al. Integration of preoperative anatomic and metabolic physiologic imaging of newly diagnosed glioma. *J Neurooncol* 2009;92(3):401–415.
57. Chawla S, Zhang Y, Wang S, et al. Proton magnetic resonance spectroscopy in differentiating glioblastomas from primary cerebral lymphomas and brain metastases. *J Comput Assist Tomogr* 2010;34(6):836–841.
58. Wijnen JP, Idema AJ, Stawicki M, et al. Quantitative short echo time <sup>1</sup>H MRSI of the peripheral edematous region of human brain tumors in the differentiation between

- glioblastoma, metastasis, and meningioma. *J Magn Reson Imaging* 2012;36(5):1072–1082.
59. Al-Okaili RN, Krejza J, Woo JH, et al. Intraaxial brain masses: MR imaging–based diagnostic strategy—initial experience. *Radiology* 2007;243(2):539–550.
  60. Hock A, Henning A, Boesiger P, Kollias SS. <sup>1</sup>H-MR spectroscopy in the human spinal cord. *AJNR Am J Neuroradiol* 2013;34(9):1682–1689.
  61. Steffen-Smith EA, Shih JH, Hipp SJ, Bent R, Warren KE. Proton magnetic resonance spectroscopy predicts survival in children with diffuse intrinsic pontine glioma. *J Neurooncol* 2011;105(2):365–373.
  62. Bliuml S, Panigrahy A, Laskov M, et al. Elevated citrate in pediatric astrocytomas with malignant progression. *Neurooncol* 2011;13(10):1107–1117.
  63. Wilson M, Cummins CL, Macpherson L, et al. Magnetic resonance spectroscopy metabolite profiles predict survival in paediatric brain tumours. *Eur J Cancer* 2013;49(2):457–464.
  64. Einstein DB, Wessels B, Bangert B, et al. Phase II trial of radiosurgery to magnetic resonance spectroscopy-defined high-risk tumor volumes in patients with glioblastoma multiforme. *Int J Radiat Oncol Biol Phys* 2012;84(3):668–674.
  65. Stadlbauer A, Moser E, Gruber S, et al. Improved delineation of brain tumors: an automated method for segmentation based on pathologic changes of <sup>1</sup>H-MR-SI metabolites in gliomas. *Neuroimage* 2004;23(2):454–461.
  66. Kallenberg K, Bock HC, Helms G, et al. Untreated glioblastoma multiforme: increased myo-inositol and glutamine levels in the contralateral cerebral hemisphere at proton MR spectroscopy. *Radiology* 2009;253(3):805–812.
  67. Scheenen TW, Klomp DW, Wijnen JP, Heerschap A. Short echo time <sup>1</sup>H-MRSI of the human brain at 3T with minimal chemical shift displacement errors using adiabatic refocusing pulses. *Magn Reson Med* 2008;59(1):1–6.
  68. Pamir MN, Özdoğan K, Dinçer A, Yıldız E, Peker S, Özek MM. First intraoperative, shared-resource, ultrahigh-field 3-Tesla magnetic resonance imaging system and its application in low-grade glioma resection. *J Neurosurg* 2010;112(1):57–69.
  69. Fink JR, Carr RB, Matsusue E, et al. Comparison of 3 Tesla proton MR spectroscopy, MR perfusion and MR diffusion for distinguishing glioma recurrence from post-treatment effects. *J Magn Reson Imaging* 2012;35(1):56–63.
  70. Murphy PS, Viviers L, Abson C, et al. Monitoring temozolomide treatment of low-grade glioma with proton magnetic resonance spectroscopy. *Br J Cancer* 2004;90(4):781–786.
  71. Matsusue E, Fink JR, Rockhill JK, Ogawa T, Maravilla KR. Distinction between glioma progression and post-radiation change by combined physiologic MR imaging. *Neuroradiology* 2010;52(4):297–306.
  72. Prat R, Galeano I, Lucas A, et al. Relative value of magnetic resonance spectroscopy, magnetic resonance perfusion, and 2-(<sup>18</sup>F) fluoro-2-deoxy-D-glucose positron emission tomography for detection of recurrence or grade increase in gliomas. *J Clin Neurosci* 2010;17(1):50–53.
  73. Hüppi PS, Posse S, Lazeyras F, Burri R, Bossi E, Herschkowitz N. Magnetic resonance in preterm and term newborns: <sup>1</sup>H-spectroscopy in developing human brain. *Pediatr Res* 1991;30(6):574–578.
  74. van der Knaap MS, van der Grond J, van Rijen PC, Faber JA, Valk J, Willemse K. Age-dependent changes in localized proton and phosphorus MR spectroscopy of the brain. *Radiology* 1990;176(2):509–515.
  75. Hanefeld F, Bauer HJ, Christen HJ, Kruse B, Bruhn H, Frahm J. Multiple sclerosis in childhood: report of 15 cases. *Brain Dev* 1991;13(6):410–416.
  76. Lodygensky GA, Menache CC, Hüppi PS. Magnetic resonance imaging's role in the care of the infant at risk for brain injury. In: Perlman JM, ed. *Neurology: neonatology questions and controversies*. 2nd ed. Amsterdam, the Netherlands: Elsevier, 2013.
  77. Hanrahan JD, Cox IJ, Edwards AD, et al. Persistent increases in cerebral lactate concentration after birth asphyxia. *Pediatr Res* 1998;44(3):304–311.
  78. Azzopardi DV, Strohm B, Edwards AD, et al. Moderate hypothermia to treat perinatal asphyxial encephalopathy. *N Engl J Med* 2009;361(14):1349–1358.
  79. van der Knaap MS, Pouwels PJ. Magnetic resonance spectroscopy: basic principles and application in white matter disorders. In: van der Knaap MS, Valk J, eds. *Magnetic resonance of myelination and myelin disorders*. 3rd ed. Berlin, Germany: Springer, 2005; 859–880.
  80. Frahm J, Hanefeld F. Localized proton magnetic resonance spectroscopy of brain disorders in childhood. In: Bachelard HS, ed. *Magnetic resonance spectroscopy and imaging in neurochemistry*. New York, NY: Plenum, 1997; 329–402.
  81. Engelke U, Moolenaar S, Hoenderop S, et al. Handbook of <sup>1</sup>H NMR spectroscopy in inborn errors of metabolism: body fluid NMR spectroscopy and in vivo MR spectroscopy. 2nd ed. Heilbronn, Germany: SPS Verlagsgesellschaft, 2007.
  82. Heindel W, Kugel H, Roth B. Noninvasive detection of increased glycine content by proton MR spectroscopy in the brains of two infants with nonketotic hyperglycinemia. *AJNR Am J Neuroradiol* 1993;14(3):629–635.
  83. Detre JA, Wang ZY, Bogdan AR, et al. Regional variation in brain lactate in Leigh syndrome by localized <sup>1</sup>H magnetic resonance spectroscopy. *Ann Neurol* 1991;29(2):218–221.
  84. Wilichowski E, Pouwels PJ, Frahm J, Hanefeld F. Quantitative proton magnetic resonance spectroscopy of cerebral metabolic disturbances in patients with MELAS. *Neuropediatrics* 1999;30(5):256–263.
  85. Bruhn H, Kruse B, Korenke GC, et al. Proton NMR spectroscopy of cerebral metabolic alterations in infantile peroxisomal disorders. *J Comput Assist Tomogr* 1992;16(3):335–344.
  86. Zand DJ, Simon EM, Pulitzer SB, et al. In vivo pyruvate detected by MR spectroscopy in neonatal pyruvate dehydrogenase deficiency. *AJNR Am J Neuroradiol* 2003;24(7):1471–1474.
  87. Ghezzi D, Goffrini P, Uziel G, et al. SDHAF1, encoding a LYR complex-II specific assembly factor, is mutated in SDH-defective infantile leukoencephalopathy. *Nat Genet* 2009;41(6):654–656.
  88. Ohlenbusch A, Edvardson S, Skorpen J, et al. Leukoencephalopathy with accumulated succinate is indicative of SDHAF1 related complex II deficiency. *Orphanet J Rare Dis* 2012;7(1):69.
  89. Manley BJ, Sokol J, Cheong JL. Intracerebral blood and MRS in neonatal nonketotic hyperglycinemia. *Pediatr Neurol* 2010;42(3):219–222.
  90. Austin SJ, Connelly A, Gadian DG, Benton JS, Brett EM. Localized <sup>1</sup>H NMR spectroscopy in Canavan's disease: a report of two cases. *Magn Reson Med* 1991;19(2):439–445.
  91. Mercimek-Mahmutoglu S, Stöckler-Ipsiroglu S, Salomons GS. Creatine deficiency syndromes. *GeneReviews* 2009. <http://www.ncbi.nlm.nih.gov/books/NBK3794/>.

- Updated August 18, 2011. Accessed April 27, 2012.
92. Stöckler S, Hanefeld F, Frahm J. Creatine replacement therapy in guanidinoacetate methyltransferase deficiency, a novel inborn error of metabolism. *Lancet* 1996;348(9030):789–790.
  93. Ndika JD, Johnston K, Barkovich JA, et al. Developmental progress and creatine restoration upon long-term creatine supplementation of a patient with arginine:glycine amidinotransferase deficiency. *Mol Genet Metab* 2012;106(1):48–54.
  94. van de Kamp JM, Pouwels PJ, Aarsen FK, et al. Long-term follow-up and treatment in nine boys with X-linked creatine transporter defect. *J Inher Metab Dis* 2012;35(1):141–149.
  95. Bizzi A, Bugiani M, Salomons GS, et al. X-linked creatine deficiency syndrome: a novel mutation in creatine transporter gene *SLC6A8*. *Ann Neurol* 2002;52(2):227–231.
  96. Wiame E, Tyteca D, Pierrot N, et al. Molecular identification of aspartate *N*-acetyltransferase and its mutation in hypoacetylaspartia. *Biochem J* 2010;425(1):127–136.
  97. Martin E, Capone A, Schneider J, Hennig J, Thiel T. Absence of *N*-acetylaspartate in the human brain: impact on neurospectroscopy? *Ann Neurol* 2001;49(4):518–521.
  98. Pouwels PJ, Brockmann K, Kruse B, et al. Regional age dependence of human brain metabolites from infancy to adulthood as detected by quantitative localized proton MRS. *Pediatr Res* 1999;46(4):474–485.
  99. Davison JE, Hendriks CJ, Sun Y, Davies NP, Gissen P, Peet AC. Quantitative in vivo brain magnetic resonance spectroscopic monitoring of neurological involvement in mucopolysaccharidosis type II (Hunter syndrome). *J Inher Metab Dis* 2010;33(Suppl 3):395–399.
  100. Davison JE, Davies NP, Wilson M, et al. MR spectroscopy-based brain metabolite profiling in propionic acidemia: metabolic changes in the basal ganglia during acute decompensation and effect of liver transplantation. *Orphanet J Rare Dis* 2011;6:19.
  101. Langlois JA, Rutland-Brown W, Thomas KE. The incidence of traumatic brain injury among children in the United States: differences by race. *J Head Trauma Rehabil* 2005;20(3):229–238.
  102. Aaen GS, Holshouser BA, Sheridan C, et al. Magnetic resonance spectroscopy predicts outcomes for children with nonaccidental trauma. *Pediatrics* 2010;125(2):295–303.
  103. Kreis R, Arciniegua E, Ernst T, Shonk TK, Flores R, Ross BD. Hypoxic encephalopathy after near-drowning studied by quantitative <sup>1</sup>H-magnetic resonance spectroscopy. *J Clin Invest* 1996;97(5):1142–1154.
  104. Bizzi A, Castelli G, Bugiani M, et al. Classification of childhood white matter disorders using proton MR spectroscopic imaging. *AJNR Am J Neuroradiol* 2008;29(7):1270–1275.
  105. van der Voorn JP, Pouwels PJ, Hart AA, et al. Childhood white matter disorders: quantitative MR imaging and spectroscopy. *Radiology* 2006;241(2):510–517.
  106. Cartier N, Aubourg P. Hematopoietic stem cell gene therapy in Hurler syndrome, globoid cell leukodystrophy, metachromatic leukodystrophy and X-adrenoleukodystrophy. *Curr Opin Mol Ther* 2008;10(5):471–478.
  107. Eichler FS, Barker PB, Cox C, et al. Proton MR spectroscopic imaging predicts lesion progression on MRI in X-linked adrenoleukodystrophy. *Neurology* 2002;58(6):901–907.
  108. Wilken B, Dechent P, Brockmann K, et al. Quantitative proton magnetic resonance spectroscopy of children with adrenoleukodystrophy before and after hematopoietic stem cell transplantation. *Neuropediatrics* 2003;34(5):237–246.
  109. Kruse B, Hanefeld F, Christen HJ, et al. Alterations of brain metabolites in metachromatic leukodystrophy as detected by localized proton magnetic resonance spectroscopy in vivo. *J Neurol* 1993;241(2):68–74.
  110. Eichler F, Grodd W, Grant E, et al. Metachromatic leukodystrophy: a scoring system for brain MR imaging observations. *AJNR Am J Neuroradiol* 2009;30(10):1893–1897.
  111. i Dali C, Hanson LG, Barton NW, Fogh J, Nair N, Lund AM. Brain *N*-acetylaspartate levels correlate with motor function in metachromatic leukodystrophy. *Neurology* 2010;75(21):1896–1903.
  112. Ding XQ, Bley A, Kohlschütter A, Fiehler J, Lanfermann H. Long-term neuroimaging follow-up on an asymptomatic juvenile metachromatic leukodystrophy patient after hematopoietic stem cell transplantation: evidence of myelin recovery and ongoing brain maturation. *Am J Med Genet A* 2012;158A(1):257–260.
  113. Sajja BR, Wolinsky JS, Narayana PA. Proton magnetic resonance spectroscopy in multiple sclerosis. *Neuroimaging Clin N Am* 2009;19(1):45–58.
  114. Davie CA, Hawkins CP, Barker GJ, et al. Detection of myelin breakdown products by proton magnetic resonance spectroscopy. *Lancet* 1993;341(8845):630–631.
  115. Hannoun S, Bagory M, Durand-Dubief F, et al. Correlation of diffusion and metabolic alterations in different clinical forms of multiple sclerosis. *PLoS ONE* 2012;7(3):e32525.
  116. Vrenken H, Barkhof F, Uitdehaag BM, Castelijns JA, Polman CH, Pouwels PJ. MR spectroscopic evidence for glial increase but not for neuro-axonal damage in MS normal-appearing white matter. *Magn Reson Med* 2005;53(2):256–266.
  117. De Stefano N, Narayanan S, Francis GS, et al. Evidence of axonal damage in the early stages of multiple sclerosis and its relevance to disability. *Arch Neurol* 2001;58(1):65–70.
  118. Tartaglia MC, Narayanan S, De Stefano N, et al. Choline is increased in pre-lesional normal appearing white matter in multiple sclerosis. *J Neurol* 2002;249(10):1382–1390.
  119. De Stefano N, Filippi M, Miller D, et al. Guidelines for using proton MR spectroscopy in multicenter clinical MS studies. *Neurology* 2007;69(20):1942–1952.
  120. de Graaf WL, Kilsdonk ID, Lopez-Soriano A, et al. Clinical application of multi-contrast 7-T MR imaging in multiple sclerosis: increased lesion detection compared to 3 T confined to grey matter. *Eur Radiol* 2013;23(2):528–540.
  121. Bizzi A, Uluğ AM, Crawford TO, et al. Quantitative proton MR spectroscopic imaging in acute disseminated encephalomyelitis. *AJNR Am J Neuroradiol* 2001;22(6):1125–1130.
  122. Chang KH, Song IC, Kim SH, et al. In vivo single-voxel proton MR spectroscopy in intracranial cystic masses. *AJNR Am J Neuroradiol* 1998;19(3):401–405.
  123. Agarwal M, Chawla S, Husain N, Jaggi RS, Husain M, Gupta RK. Higher succinate than acetate levels differentiate cerebral degenerating cysticerci from anaerobic abscesses on in-vivo proton MR spectroscopy. *Neuroradiology* 2004;46(3):211–215.
  124. Sturrock A, Laule C, Decolgon J, et al. Magnetic resonance spectroscopy biomarkers in premanifest and early Huntington disease. *Neurology* 2010;75(19):1702–1710.
  125. Kantarci K, Jack CR Jr, Xu YC, et al. Regional metabolic patterns in mild cognitive impairment and Alzheimer's disease: a <sup>1</sup>H MRS study. *Neurology* 2000;55(2):210–217.

126. Adalsteinsson E, Sullivan EV, Kleinhans N, Spielman DM, Pfefferbaum A. Longitudinal decline of the neuronal marker *N*-acetyl aspartate in Alzheimer's disease. *Lancet* 2000;355(9216):1696–1697.
127. Öz G, Hutter D, Tkáč I, et al. Neurochemical alterations in spinocerebellar ataxia type 1 and their correlations with clinical status. *Mov Disord* 2010;25(9):1253–1261.
128. Unschuld PG, Edden RA, Carass A, et al. Brain metabolite alterations and cognitive dysfunction in early Huntington's disease. *Mov Disord* 2012;27(7):895–902.
129. Kantarci K, Weigand SD, Petersen RC, et al. Longitudinal <sup>1</sup>H MRS changes in mild cognitive impairment and Alzheimer's disease. *Neurobiol Aging* 2007;28(9):1330–1339.
130. Griffith HR, Stewart CC, den Hollander JA. Proton magnetic resonance spectroscopy in dementias and mild cognitive impairment. *Int Rev Neurobiol* 2009;84:105–131.
131. Rupsingh R, Borrie M, Smith M, Wells JL, Bartha R. Reduced hippocampal glutamate in Alzheimer disease. *Neurobiol Aging* 2011;32(5):802–810.
132. Öz G, Iltis I, Hutter D, Thomas W, Bushara KO, Gomez CM. Distinct neurochemical profiles of spinocerebellar ataxias 1, 2, 6, and cerebellar multiple system atrophy. *Cerebellum* 2011;10(2):208–217.
133. Miller BL, Moats RA, Shonk T, Ernst T, Woolley S, Ross BD. Alzheimer disease: depiction of increased cerebral myo-inositol with proton MR spectroscopy. *Radiology* 1993;187(2):433–437.
134. Ross BD, Bluml S, Cowan R, Danielsen E, Farrow N, Tan J. In vivo MR spectroscopy of human dementia. *Neuroimaging Clin N Am* 1998;8(4):809–822.
135. Godbolt AK, Waldman AD, MacManus DG, et al. MRS shows abnormalities before symptoms in familial Alzheimer disease. *Neurology* 2006;66(5):718–722.
136. Kantarci K, Boeve BF, Wszolek ZK, et al. MRS in presymptomatic MAPT mutation carriers: a potential biomarker for tau-mediated pathology. *Neurology* 2010;75(9):771–778.
137. Krishnan KR, Charles HC, Doraiswamy PM, et al. Randomized, placebo-controlled trial of the effects of donepezil on neuronal markers and hippocampal volumes in Alzheimer's disease. *Am J Psychiatry* 2003;160(11):2003–2011.
138. Bartha R, Smith M, Rupsingh R, Rylett J, Wells JL, Borrie MJ. High field <sup>1</sup>H MRS of the hippocampus after donepezil treatment in Alzheimer disease. *Prog Neuropsychopharmacol Biol Psychiatry* 2008;32(3):786–793.
139. Penner J, Rupsingh R, Smith M, Wells JL, Borrie MJ, Bartha R. Increased glutamate in the hippocampus after galantamine treatment for Alzheimer disease. *Prog Neuropsychopharmacol Biol Psychiatry* 2010;34(1):104–110.
140. Kwan P, Brodie MJ. Early identification of refractory epilepsy. *N Engl J Med* 2000;342(5):314–319.
141. Del Felice A, Beghi E, Boero G, et al. Early versus late remission in a cohort of patients with newly diagnosed epilepsy. *Epilepsia* 2010;51(1):37–42.
142. Wiebe S, Jetté N. Epilepsy surgery utilization: who, when, where, and why? *Curr Opin Neurol* 2012;25(2):187–193.
143. Englot DJ, Wang DD, Rolston JD, Shih TT, Chang EF. Rates and predictors of long-term seizure freedom after frontal lobe epilepsy surgery: a systematic review and meta-analysis. *J Neurosurg* 2012;116(5):1042–1048.
144. Siesjö BK. Brain energy metabolism. London, England: Wiley, 1978.
145. Pan JW, Williamson A, Cavus I, et al. Neuro-metabolism in human epilepsy. *Epilepsia* 2008;49(Suppl 3):31–41.
146. Capizzano AA, Vermathen P, Laxer KD, et al. Temporal lobe epilepsy: qualitative reading of <sup>1</sup>H MR spectroscopic images for pre-surgical evaluation. *Radiology* 2001;218(1):144–151.
147. Connelly A, Jackson GD, Duncan JS, King MD, Gadian DG. Magnetic resonance spectroscopy in temporal lobe epilepsy. *Neurology* 1994;44(8):1411–1417.
148. Simister RJ, McLean MA, Barker GJ, Duncan JS. Proton MR spectroscopy of metabolite concentrations in temporal lobe epilepsy and effect of temporal lobe resection. *Epilepsy Res* 2009;83(2-3):168–176.
149. Maudsley AA, Domenig C, Ramsay RE, Bowen BC. Application of volumetric MR spectroscopic imaging for localization of neocortical epilepsy. *Epilepsy Res* 2010;88(2-3):127–138.
150. Pan JW, Duckrow RB, Spencer DD, Avdievich NI, Hetherington HP. Selective homonuclear polarization transfer for spectroscopic imaging of GABA at 7T. *Magn Reson Med* 2013;69(2):310–316.
151. Willmann O, Wennberg R, May T, Woermann FG, Pohlmann-Eden B. The role of <sup>1</sup>H magnetic resonance spectroscopy in pre-operative evaluation for epilepsy surgery: a meta-analysis. *Epilepsy Res* 2006;71(2-3):149–158.
152. Fountas KN, Tsougos I, Gotsis ED, Giannakodimos S, Smith JR, Kapsalaki EZ. Temporal pole proton preoperative magnetic resonance spectroscopy in patients undergoing surgery for mesial temporal sclerosis. *Neurosurg Focus* 2012;32(3):E3.
153. Pan JW, Avdievich N, Hetherington HP. J-refocused coherence transfer spectroscopic imaging at 7 T in human brain. *Magn Reson Med* 2010;64(5):1237–1246.
154. Cross JH, Connelly A, Jackson GD, Johnson CL, Neville BG, Gadian DG. Proton magnetic resonance spectroscopy in children with temporal lobe epilepsy. *Ann Neurol* 1996;39(1):107–113.
155. González RG. Clinical MRI of acute ischemic stroke. *J Magn Reson Imaging* 2012;36(2):259–271.
156. van der Toorn A, Verheul HB, Berkelbach van der Sprenkel JW, Tulleken CA, Nicolay K. Changes in metabolites and tissue water status after focal ischemia in cat brain assessed with localized proton MR spectroscopy. *Magn Reson Med* 1994;32(6):685–691.
157. Sager TN, Laursen H, Hansen AJ. Changes in *N*-acetyl-aspartate content during focal and global brain ischemia of the rat. *J Cereb Blood Flow Metab* 1995;15(4):639–646.
158. Saunders DE. MR spectroscopy in stroke. *Br Med Bull* 2000;56(2):334–345.
159. Parsons MW, Li T, Barber PA, et al. Combined <sup>1</sup>H MR spectroscopy and diffusion-weighted MRI improves the prediction of stroke outcome. *Neurology* 2000;55(4):498–505.
160. Petroff OA, Graham GD, Blamire AM, et al. Spectroscopic imaging of stroke in humans: histopathology correlates of spectral changes. *Neurology* 1992;42(7):1349–1354.
161. Klijn CJ, Kappelle LJ, van der Grond J, Algra A, Tulleken CA, van Gijn J. Magnetic resonance techniques for the identification of patients with symptomatic carotid artery occlusion at high risk of cerebral ischemic events. *Stroke* 2000;31(12):3001–3007.
162. Emir UE, Tuite PJ, Öz G. Elevated pontine and putamenal GABA levels in mild-moderate Parkinson disease detected by 7 Tesla proton MRS. *PLoS ONE* 2012;7(1):e30918.
163. Scheenen TW, Heerschap A, Klomp DW. Towards <sup>1</sup>H-MRSI of the human brain at 7T with slice-selective adiabatic refocusing pulses. *MAGMA* 2008;21(1-2):95–101.
164. Kreis R. Issues of spectral quality in clinical <sup>1</sup>H-magnetic resonance spectroscopy and

- a gallery of artifacts. *NMR Biomed* 2004;17(6):361–381.
165. Soher BJ, Semanchuk P, Todd D, Steinberg J, Young K. Vespa: integrated applications for RF pulse design, spectral simulation and MRS data analysis [abstr]. In: Proceedings of the Nineteenth Meeting of the International Society for Magnetic Resonance in Medicine. Berkeley, Calif: International Society for Magnetic Resonance in Medicine, 2011; 1410.
  166. Provencher SW. Automatic quantitation of localized in vivo  $^1\text{H}$  spectra with LCModel. *NMR Biomed* 2001;14(4):260–264.
  167. Scheidegger O, Wingeier K, Stefan D, et al. Optimized quantitative magnetic resonance spectroscopy for clinical routine. *Magn Reson Med* 2013;70(1):25–32.
  168. Gu M, Kim DH, Mayer D, Sullivan EV, Pfefferbaum A, Spielman DM. Reproducibility study of whole-brain  $^1\text{H}$  spectroscopic imaging with automated quantification. *Magn Reson Med* 2008;60(3):542–547.
  169. Schirmer T, Auer DP. On the reliability of quantitative clinical magnetic resonance spectroscopy of the human brain. *NMR Biomed* 2000;13(1):28–36.
  170. Hammen T, Stadlbauer A, Tomandl B, et al. Short TE single-voxel  $^1\text{H}$ -MR spectroscopy of hippocampal structures in healthy adults at 1.5 Tesla: how reproducible are the results? *NMR Biomed* 2005;18(3):195–201.
  171. Li BS, Babb JS, Soher BJ, Maudsley AA, Gonen O. Reproducibility of 3D proton spectroscopy in the human brain. *Magn Reson Med* 2002;47(3):439–446.
  172. Wijnen JP, van Asten JJ, Klomp DW, et al. Short echo time  $^1\text{H}$  MRSI of the human brain at 3T with adiabatic slice-selective refocusing pulses: reproducibility and variance in a dual center setting. *J Magn Reson Imaging* 2010;31(1):61–70.
  173. Gasparovic C, Bedrick EJ, Mayer AR, et al. Test-retest reliability and reproducibility of short-echo-time spectroscopic imaging of human brain at 3T. *Magn Reson Med* 2011;66(2):324–332.
  174. Terpstra M, Emir UE, Eberly LE, Öz G. Test-retest repeatability of human neurochemical profiles measured at 3 versus 7 T [abstr]. In: Proceedings of the Twentieth Meeting of the International Society for Magnetic Resonance in Medicine. Berkeley, Calif: International Society for Magnetic Resonance in Medicine, 2012; 1739.
  175. Öz G, Tkáč I. Short-echo, single-shot, full-intensity proton magnetic resonance spectroscopy for neurochemical profiling at 4 T: validation in the cerebellum and brainstem. *Magn Reson Med* 2011;65(4):901–910.
  176. Smith IC, Somorjai RL. Deriving biomedical diagnostics from NMR spectroscopic data. *Biophys Rev* 2011;3(1):47–52.
  177. Somorjai RL. Creating robust, reliable, clinically relevant classifiers from spectroscopic data. *Biophys Rev* 2009;1(4):201–211.